

H. E. Layton, John M. Davies, Giovanni Casotti and Eldon J. Braun
Am J Physiol Renal Physiol 279:1139-1160, 2000.

You might find this additional information useful...

This article cites 65 articles, 24 of which you can access free at:

<http://ajprenal.physiology.org/cgi/content/full/279/6/F1139#BIBL>

This article has been cited by 2 other HighWire hosted articles:

A region-based mathematical model of the urine concentrating mechanism in the rat outer medulla. I. Formulation and base-case results

A. T. Layton and H. E. Layton

Am J Physiol Renal Physiol, December 1, 2005; 289 (6): F1346-F1366.

[Abstract] [Full Text] [PDF]

Two modes for concentrating urine in rat inner medulla

A. T. Layton, T. L. Pannabecker, W. H. Dantzler and H. E. Layton

Am J Physiol Renal Physiol, October 1, 2004; 287 (4): F816-F839.

[Abstract] [Full Text] [PDF]

Medline items on this article's topics can be found at <http://highwire.stanford.edu/lists/artbytopic.dtl> on the following topics:

Physiology .. Kidneys

Physiology .. Loop of Henle

Physiology .. Galliformes

Computer Science .. Mathematical Modeling

Updated information and services including high-resolution figures, can be found at:

<http://ajprenal.physiology.org/cgi/content/full/279/6/F1139>

Additional material and information about *AJP - Renal Physiology* can be found at:

<http://www.the-aps.org/publications/ajprenal>

This information is current as of July 31, 2007 .

Mathematical model of an avian urine concentrating mechanism

H. E. LAYTON,¹ JOHN M. DAVIES,¹ GIOVANNI CASOTTI,² AND ELDON J. BRAUN³

¹Department of Mathematics, Duke University, Durham, North Carolina 27708-0320; ²Department of Biology, West Chester University, West Chester, Pennsylvania 19383; and ³Department of Physiology, University of Arizona Health Sciences Center, Tucson, Arizona 85724-5051

Received 1 November 1999; accepted in final form 20 July 2000

Layton, H. E., John M. Davies, Giovanni Casotti, and Eldon J. Braun. Mathematical model of an avian urine concentrating mechanism. *Am J Physiol Renal Physiol* 279: F1139–F1160, 2000.—A mathematical model was used to investigate how concentrated urine is produced within the medullary cones of the quail kidney. Model simulations were consistent with a concentrating mechanism based on single-solute countercurrent multiplication and on NaCl cycling from ascending to descending limbs of loops of Henle. The model predicted a urine-to-plasma (U/P) osmolality ratio of ~2.26, a value consistent with maximum avian U/P osmolality ratios. Active NaCl transport from descending limb prebend thick segments contributed 70% of concentrating capability. NaCl entry and water extraction provided 80 and 20%, respectively, of the concentrating effect in descending limb flow. Parameter studies indicated that urine osmolality is sensitive to the rate of fluid entry into descending limbs and collecting ducts at the cone base. Parameter studies also indicated that the energetic cost of concentrating urine is sensitive to loop of Henle population as a function of medullary depth: as the fraction of loops reaching the cone tip increased above anatomic values, urine osmolality increased only marginally, and, ultimately, urine osmolality decreased. kidney; countercurrent multiplication; *Callipepla gambelii*; *Coturnix coturnix*

BIRDS, LIKE MAMMALS, can produce hypertonic urine when body water must be conserved to maintain a stable blood plasma osmolality. However, this capability is limited in birds compared with mammals: urine-to-plasma (U/P) osmolality ratios seldom exceed 2 in birds (20), whereas most mammals can produce ratios of ≥ 4 (2).

Hypertonic urine is produced in the medullary cones of the avian kidney (16, 66). The number of medullary cones per kidney may range over two orders of magnitude, from tens to thousands, as a function of body mass (20). Each cone may contain up to several hundred loops of Henle (20), and each cone contains a coalescing system of collecting ducts (CDs) (3). The populations of loops of Henle and CDs decrease rapidly as a function of medullary cone length; in Gambel's quail (*Callipepla gambelii*), the number of these tu-

bules can be well approximated by exponentially decreasing functions (11). Only a fraction of the nephrons in each avian kidney have loops of Henle; most nephrons are loopless, like those in reptiles. In Gambel's quail ~10% of nephrons have loops.

Experimental and theoretical studies have supported the hypothesis that countercurrent multiplication produces concentrated urine in the mammalian renal medulla (26, 40, 63). According to this hypothesis, a small osmotic pressure difference between adjacent renal tubules is multiplied (or augmented) by countercurrent (i.e., antiparallel) fluid flow, resulting in a large increase in osmotic pressure along the corticomedullary axis. The small osmotic pressure difference, which is perpendicular to the flow directions, is called the "single effect." The source of the single effect in the outer medulla is the vigorous active transport of NaCl across the thick epithelium of the ascending limbs (ALs); that transport is driven by $\text{Na}^+\text{-K}^+\text{-ATPase}$ pumps in the basolateral membranes of the cells (21). The transepithelial osmotic gradient so generated can be sustained because of the low permeability of the thick AL epithelium to water and NaCl (63). However, experiments indicate that the thin ALs of the inner medulla can neither generate nor sustain a significant transepithelial NaCl gradient, and no generally satisfactory explanation has been advanced for how the inner medulla functions in the concentrating mechanism (12).

In the avian kidney, the present evidence indicates that all ALs are thick limbs. As in mammals, the thick AL epithelium in birds actively transports NaCl from the tubular lumen to the interstitium, and in the Japanese quail (*Coturnix coturnix*) the thick limb epithelium appears to have a low permeability to water and NaCl (49, 50). In addition, each avian loop of Henle has a prebend thick descending segment [or, alternatively, prebend enlargement (PBE)], of variable length, which is contiguous with the AL and is believed to have epithelial transport characteristics similar to those of the avian AL (6, 11). Thin descending limbs (DLs) in the Japanese quail have low water permeability, but

Address for reprint requests and other correspondence: H. E. Layton, Dept. of Mathematics, Duke University, Box 90320, Durham, NC 27708-0320 (E-mail: layton@math.duke.edu).

The costs of publication of this article were defrayed in part by the payment of page charges. The article must therefore be hereby marked "advertisement" in accordance with 18 U.S.C. Section 1734 solely to indicate this fact.

the limbs are highly permeable to Na^+ and Cl^- relative to mammalian DLs (51). CDs in the Japanese quail appear to have a low osmotic water permeability, compared with mammalian CDs under the influence of antidiuretic hormone, and the avian ducts appear to be little affected by arginine vasotocin, the avian antidiuretic hormone (52). Little is known about the morphological or transport properties of the medullary cone vasculature.

On the basis of the counterflow configuration of the tubules in the medullary cone and the finding of an NaCl corticomedullary gradient in chicken and turkey, Skadhauge and Schmidt-Nielsen (66) proposed that birds produce concentrated urine by means of countercurrent multiplication. On the basis of the subsequent elucidation of the transport characteristics of the tubular epithelium (chiefly in the Japanese quail), Nishimura et al. (51) set forth a specific hypothesis for the operation of the avian concentrating mechanism as a countercurrent multiplier system. They proposed that active transepithelial transport of NaCl from the ALs is the source of the single effect of the avian countercurrent mechanism, that thin DL fluid osmolality is increased principally by NaCl entry via transepithelial diffusion, and that this NaCl is then, in turn, delivered by advection (i.e., the motion of fluid, or the solute carried by the fluid, along the tubular lumen) to thick AL lumens, where it is again subject to active transepithelial transport. They hypothesized that this process of single-solute cycling, in conjunction with a transport cascade resulting from loops of Henle of various lengths reaching to different depths within the medullary cone, contributes to the concentrating effect. Concentrated urine was assumed to form by the near-osmotic equilibration of CD fluid with the medullary cone interstitium. As in the outer medulla of the mammalian kidney, the thick ALs would carry fluid that is dilute, with respect to blood plasma, from the medullary cone into the cortex.

In mammals, nitrogen is excreted in urea, and urea is believed to have an important role in the mammalian urine concentrating mechanism (17, 62). In birds, however, nitrogen is excreted mostly in uric acid, which is incorporated in small, spherical structures that form a stable hydrophobic suspension; that suspension is an osmotically inactive component of avian urine (7, 10). Urea is found in low concentrations in the avian medullary cone and is therefore thought to have no significant role in the avian concentrating mechanism (66).

In this study we describe a mathematical model of the avian urine concentrating mechanism, as found in quail, and we present simulation results based on that model. For a "base-case" simulation, we used mostly morphological and transepithelial transport parameters measured in Gambel's quail and in the Japanese quail. Simulations based on the model were used to predict intratubular concentrations, intratubular flows, and transepithelial transport rates as a function of position along the cone. By altering the parameters

of the base case, we investigated the effects of parameter values on concentrating capability and efficiency.

The model simulations tend to confirm that the medullary cone operates as a countercurrent multiplier system, much as proposed by Nishimura et al. (51). Moreover, the simulations indicate that prebend thick limbs can significantly augment concentrating capability compared with the hypothetical case where prebend thick limbs are absent. In addition, simulation results suggest an explanation for the decreasing population of loops of Henle as a function of cone depth: because of the decrease in total CD flow (as ducts traverse the medullary cone) and the resulting decrease in osmotic load, additional loops, exceeding the number reported and reaching deep into the cone, would have little effect on final urine osmolality. Thus there would be diminishing returns for the additional solute that would be transported across thick ALs, and additional long loops would serve only to increase the energetic cost of producing hypertonic urine.

In a strict sense, the results of this study are applicable only to the concentrating mechanism as found in species similar to the quail, and thus this is a study of "an" avian concentrating mechanism. Yet, because most avian species so far studied have medullary cone anatomy that is substantially similar to that of the quail and because our simulation results predict U/P osmolality ratios that range over the values found in many birds, our results may be representative of the avian urine concentrating mechanism in many or most avian species. However, a species exhibiting exceptions to hypotheses adopted in this study is known: the Anna's hummingbird, *Calypste anna* (9). This nectarivorous bird has only ~0.4% looped nephrons, and these looped nephrons have no thin DLs, but instead their loops of Henle have cells entirely like those of thick ALs. The kidneys of the Anna's hummingbird are unable to produce a urine more concentrated than blood plasma.

MATHEMATICAL MODEL

Model structure. A schematic diagram of the mathematical model is given in Fig. 1. The model, which is structurally similar to several previous models (42–44), uses the central core (CC) formulation introduced by Stephenson (70). In this formulation, the extratubular contents of the medulla (i.e., vasculature, interstitial spaces, and interstitial cells) are merged into a single tube, the CC, through which the loops of Henle and the CD system interact. The CC is closed at the medullary tip but is contiguous with the cortical interstitium at the corticomedullary boundary.

Because experimental evidence indicates that only one solute, NaCl, plays a significant role in the avian urine concentrating mechanism (16, 66), the model was formulated for a single solute, represented by Cl^- . Osmolalities were computed by assuming that each Cl^- ion was accompanied by a cation, assumed to be principally Na^+ .

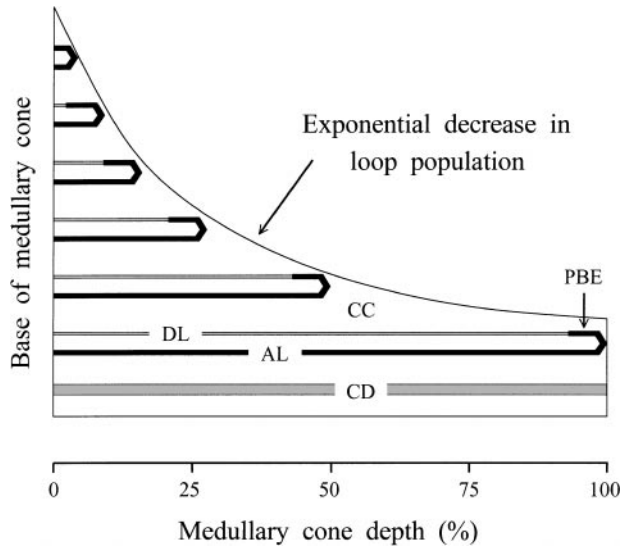


Fig. 1. Schematic diagram of model for avian medullary cone. The collecting duct (CD) system is merged into a composite CD. Descending limbs of loops of Henle (DL), ascending limbs of loops of Henle (AL), and CD interact through a common tubular compartment, the central core (CC). The number of loops decreases exponentially as a function of medullary depth, as indicated by morphological investigation (11) and suggested in this diagram by the reduced numbers of loops of Henle as a function of medullary depth; 6 representative loops are shown here, but the numerical formulation of the model uses 80 loops of Henle to approximate a continuously decreasing distribution. Each DL has a prebend enlargement (PBE) that is assumed to have the same transepithelial transport properties as ALs. In the model, loop bends are not explicitly represented; flow from each DL enters directly its associated AL.

The CD system was represented as a single tube of varying diameter, scaled according to the number of CDs reaching each medullary level. Fluid flow, Cl^- concentration, and fluid osmolality in the CC and CD system were represented by functions of position along the corticomedullary axis. The loops of Henle, which reach to different levels of the avian medullary cone, were represented in the model by a continuous, monotonically decreasing distribution of tubes (Fig. 1). The continuous distribution is constructed by formulating each dependent variable (e.g., concentration or flow rate) associated with a DL or an AL as a function of both axial position and the medullary level at which the loop of Henle turns. The continuous distribution provides detailed information about the luminal contents of individual loops of Henle and how those contents vary as a function of loop-bend depth. Moreover, this formulation allows for the representation of axial inhomogeneities in the transport properties of DLs; in particular, it allows the explicit inclusion of a prebend segment with transepithelial transport characteristics similar to those of the ALs.

The model was formulated for the medullary cone only and did not explicitly include a representation of the renal cortex. Some renal models have included additional equations describing water flows and solute concentrations in the cortical tubules that connect the ALs and the CD system (72). However, since in this report we are concerned mostly with medullary func-

tion and since knowledge of transepithelial transport in the distal tubule is less complete than for the medulla, the boundary conditions (flow rates and concentrations) were prescribed for the DLs and the composite CD at the base of the medullary cone, i.e., at the corticomedullary boundary. Analogous conditions were not required for the ALs and CC, since the flow from these tubules is normally into the cortex.

The fundamental equations for the mathematical model used here have been derived elsewhere (46, 47); however, the formulation used here differs, in that a nonzero fraction of model loops of Henle reaches the tip of the cone, in accordance with experimental findings (11). For completeness, the model equations are given in the APPENDIX.

Model parameters. In the simulation studies reported here, morphological and membrane transport parameters were varied relative to a particular base case chosen to approximate the quail medullary cone. The base-case morphological parameters were based on a medullary cone from a specimen of Gambel's quail (designated *cone 11* in Ref. 11). *Cone 11* was a typical representative of other cones within that animal, except it had the greatest length, as measured from cone base to cone tip, i.e., 3.35 mm, and it therefore provided the most detailed structural information. For the model, we used data from the deepest 3.25 mm of that cone, where the loop and CD counts were found to be nearly monotonically decreasing.

To represent the 98 loops of Henle and 28 CDs that entered the particular cone, a ratio of total loops to CDs of 98:28 was assumed at the corticomedullary boundary. The avian loops of Henle are of variable length and turn back at various levels along the medullary cone (11), with most turning back near the cone base. Similarly, the number of CDs decreases along the cone because of the successive coalescences of two ducts into one duct (3). Morphological measurements indicate that, as a function of medullary depth, the loop of Henle and CD populations decrease approximately exponentially (11). Similar patterns have been found in rat (25, 36) and rabbit (64).

A least-squares fit to the natural logarithm of the loop population measured in medullary *cone 11* in Ref. 11 showed that the fraction, w , of loops of Henle reaching to medullary depth x is well approximated by a function of the form $w(x) = e^{-3.22x/L}$, where $x = 0$ and $x = L$ correspond to the cone base and the cone tip, respectively (percent cone depth is $x/L \times 100\%$). Similarly, the fraction of CDs, w_{cd} , reaching to medullary depth x is well approximated by $w_{\text{cd}}(x) = e^{-2.88x/L}$. The continuous curves corresponding to these loop and CD fractions are shown in Fig. 2. The fractional loop distribution was used in computing the composite fluxes from the aggregate of loops of Henle, and the fractional number of CDs was used in scaling the composite CD.

Luminal loop of Henle and CD diameters, based on data from the same medullary cone, are given in Table 1. The thin DL diameter given in Table 1 is an average over all thin DLs at all depths. The thick AL diameter at the cone base ($x = 0$) was based on a least-squares

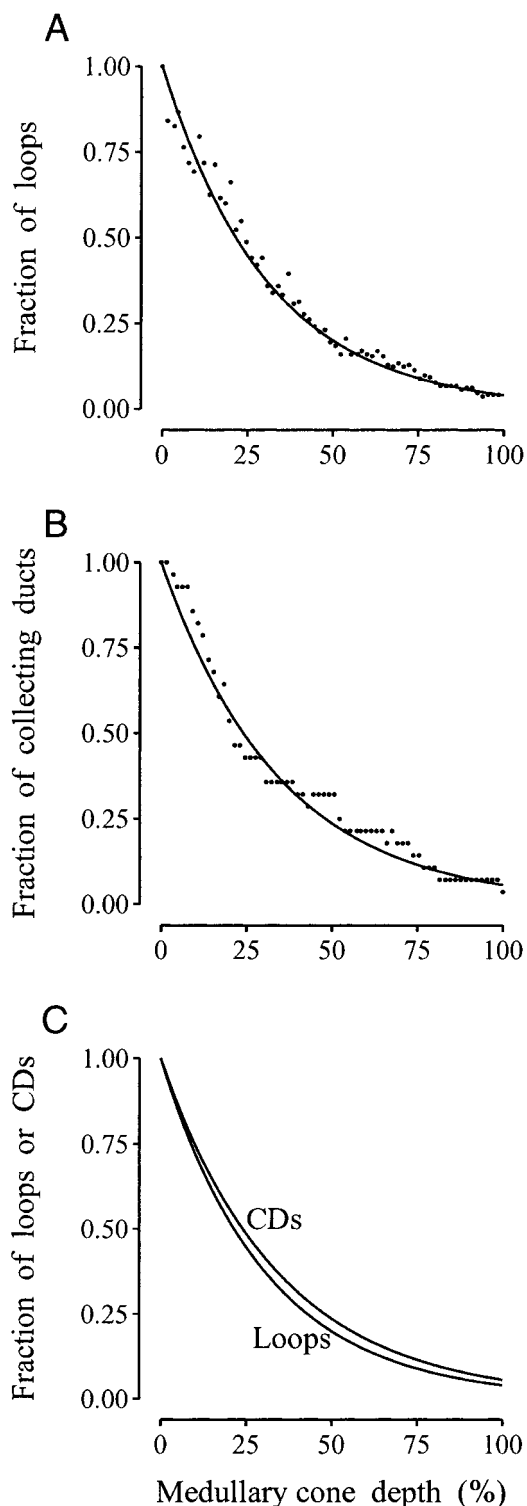


Fig. 2. A: fraction of loops of Henle as a function of cone depth. ●, Experimental counts of loops of Henle, divided by total loops at cone base (data from the study published as Ref. 11); curve, approximation used in the model to give appropriate weight to loops of Henle of differing lengths. B: fraction of CDs as a function of cone depth. ●, Experimental counts of CDs divided by total number of CDs at cone base; curve, approximation used in the model to give the appropriate weight to surface area of composite CD. C: comparison of fractional populations of loops of Henle and CDs (curves from A and B). The pattern of similar exponential decrease exhibited by these curves suggests that CD osmotic load at each level is balanced with concentrating capacity available from loops of Henle at that level.

Table 1. Inner diameters of tubules

Segment	Diameter, μm
Thin DL	6.81
Thick AL	
Cone base	9.55
Cone tip	11.4
CD	
Cone base	19.1
Cone tip	66.7

DL and AL, descending and ascending limbs, respectively, of loop of Henle; CD, collecting duct.

fit to average diameters all along the cone (average diameters were measured at 50- μm intervals in Ref. 11); the thick AL value at the cone tip is an average over the loops reaching the cone tip. The CD diameter at the cone base is the average diameter over all CDs at $x = 0$; the cone tip diameter is based on the cone tip values of a least-squares fit to average diameters along the cone. The diameters used in the model at each numerical grid point were obtained from these values by smooth interpolations similar to those previously described and used in Refs. 45 and 47.

Loop of Henle diameters, as incorporated in the model, are represented by means of level curves in Fig. 4A (to facilitate comparisons, Fig. 4A is grouped with level curves of simulated quantities in RESULTS). Level curves represent functional values in the same way that elevations are specified on topographical maps: the label on each curve gives the value that the variable parameter assumes on that curve. Thus level curves provide a means for representing a three-dimensional surface in two dimensions. Loop of Henle diameters change continuously and smoothly between the level curves portrayed in Fig. 4A. In Fig. 4, A and D, the lengths of DL segments are indicated as a percentage of cone depth along the lower horizontal axis and the lengths of AL segments are indicated along the right vertical axis. Loop bends occur along the dashed diagonal line extending from the upper left to the lower right. A shaded region labeled "DL" and "AL" suggests a loop of Henle reaching about three-fourths of the way into the medulla. (See APPENDIX for more information about construction of Fig. 4.)

CD diameter, as a function of medullary cone depth, increased approximately exponentially by a fractional amount given by $e^{1.25x/L}$, where x ranges from 0 to L along the medullary axis. The CD system surface area was determined from this diameter scaling and from the number of CDs as a function of medullary depth.

The cross-sectional area of the CC, not including the tubules enclosed by the core, was taken to be $0.9w(x) + 0.1$ (where w is the fraction of loops) times the luminal cross-sectional area of a DL at the corticomedullary boundary. Thus the volume of the cross-sectional area of the CC approximates that of the aggregate DLs. However, steady-state solutions do not depend on the cross-sectional area of the CC (or of any other tubule; see APPENDIX).

Table 2. *Base-case transport properties*

Segment	P_f , $\mu\text{m/s}$	P_{Cl^-} , 10^{-5} cm/s	V_{max} , $\text{nmol}\cdot\text{cm}^{-2}\cdot\text{s}^{-1}$
Thin DL	$552 \pm 215(51)$	$116 \pm 17(51)$	0
Thick limbs	$57.2 \pm 9.4(49)$	4.32 (49)	$19.5 \pm 1.5(49)$
CD	115 (52)	1.00*	0

Values are means \pm SE. Numbers in parentheses indicate references. P_f , osmotic water permeability; P_{Cl^-} , Cl^- permeability; V_{max} , maximum active Cl^- transport rate. *Based on Na^+ permeability in rabbit outer medullary CD (73).

Our base-case transepithelial transport parameters are summarized in Table 2. To obtain transepithelial transport parameters that could be scaled according to tubular areas measured in Gambel's quail, we assumed that typical tubular areas per unit length are similar in the Japanese quail and Gambel's quail. Using this assumption, we converted transport parameter values reported per unit tubular length in the Japanese quail to values expressed per unit tubular area. Thus hydraulic conductivity in DLs of Japanese quail, which has been reported to be $83.3 \pm 32.4 \times 10^{-9} \text{ cm}^2\cdot\text{s}^{-1}\cdot\text{atm}^{-1}$ (51), corresponds to an osmotic water permeability of $552 \pm 215 \mu\text{m/s}$, when one assumes a luminal tubular diameter of $6.81 \mu\text{m}$ and a temperature of 310°K . Similarly, hydraulic conductivity in ALs of the Japanese quail has been reported to be $12.8 \pm 2.1 \times 10^{-9} \text{ cm}^2\cdot\text{s}^{-1}\cdot\text{atm}^{-1}$ (49); for a tubular diameter of $10.1 \mu\text{m}$ (the average luminal thick limb diameter), that hydraulic conductivity corresponds to an osmotic water permeability of $57.2 \pm 9.4 \mu\text{m/s}$.

Osmotic water permeability in the CD was estimated from measurements in Ref. 52, which reported an osmotic water flux of $\sim 0.396 \text{ nl}\cdot\text{min}^{-1}\cdot\text{mm}^{-1}$ with 50–200 mosmol/kgH₂O osmotic gradient along a tubule $\sim 0.430 \text{ mm}$ long. Under normal circumstances, one expects that the transepithelial osmotic gradient will be small. For an osmotic gradient of 50 mosmol/kgH₂O and an assumed inner diameter of $\sim 20 \mu\text{m}$ (typical of the initial CD of Gambel's quail), an osmotic water permeability of $115 \mu\text{m/s}$ can be calculated.

The Cl^- flux coefficient ($10^{-7} \text{ cm}^2/\text{s}$) in DLs of the Japanese quail (51) has been measured (51) to be 24.9 ± 3.6 . With the assumption of a diameter of $6.81 \mu\text{m}$, this corresponds to a permeability in standard units (10^{-5} cm/s) of 116 ± 17 . Cl^- permeability for the AL was based on the Cl^- influx coefficient measured in Ref. 49. A typical influx coefficient of $1.37 \times 10^{-7} \text{ cm}^2/\text{s}$ and an assumed diameter of $10.1 \mu\text{m}$ indicate a Cl^- permeability of ~ 4.32 . Cl^- permeability (10^{-5} cm/s) in the CD was assumed to have a value of 1, similar to the value for Na^+ (~ 0.39) reported in the rabbit outer medullary CD (73).

The active transport rate for Cl^- from the AL was based on the average efflux rate of $370.4 \pm 27.7 \text{ peq}\cdot\text{mm}^{-1}\cdot\text{min}^{-1}$ reported in Ref. 49. If one assumes an AL inner diameter of $10.1 \mu\text{m}$, this efflux rate corresponds to a flux of $19.5 \pm 1.5 \text{ nmol}\cdot\text{cm}^{-2}\cdot\text{s}^{-1}$. This flux was taken to be the maximum active transport rate; this rate is similar to those used in models of the

mammalian concentrating mechanism (45, 78), which have generally been chosen to obtain an outer medullary osmolality increase of a factor of ~ 2 . Other active transport rates in the medullary cone were assumed to be too small to have a significant role in the concentrating mechanism; consequently, they were set to zero. The Michaelis constant (K_m) was set to 40 mM (22), and reflection coefficients were everywhere set to 1 on the basis of findings in the mammalian medulla (63).

The boundary conditions for incoming flows are summarized in Table 3. Cl^- concentration entering the DLs and the CD system was set to 130 mM, consistent with measurements ($130.60 \pm 3.27 \text{ mM}$) in the proximal tubule of the European starling (41). Fluid flow rate entering DLs at the corticomedullary boundary was taken to be 5.53 nl/min , which is 35% of single-nephron glomerular filtration rate measured for long-looped nephrons in Gambel's quail (5). Fluid flow rate entering the CD system per looped nephron was taken to be 0.500 nl/min on the basis of the following considerations. Total urine flow rate from both kidneys combined, in water-deprived Gambel's quail, has been measured to be $0.15 \pm 0.1 \text{ ml/h}$ (associated urine osmolality was $637 \pm 90 \text{ mosmol/kgH}_2\text{O}$) (80). The number of looped nephrons has been estimated at 4,678 per kidney (5). Thus the rate of urine production per looped nephron is $\sim 0.27 \text{ nl/min}$. Since the avian medullary cone is reported to achieve U/P osmolality ratios approaching 2 (5, 16, 66), we assume that $\sim 45\%$ of fluid entering the CD system at the corticomedullary axis is removed along the medullary cone, resulting in a flow of $\sim 0.5 \text{ nl/min}$ entering the CD system per looped nephron. Thus the fluid load on the concentrating system is about one-tenth of the fluid rate entering the loops of Henle at the corticomedullary boundary.

Numerical calculations. Numerical approximations to steady-state solutions of the model equations were obtained via a previously developed, fully explicit dynamic method (46, 47). The numerical method was programmed in FORTRAN, and computations were performed in double-precision mode on a Sun Microsystems SPARCstation Ultra 1. In each model simulation, the numerical approximation was computed in time until the osmolality of the CD effluent was varying by <1 part in 10^{14} , the maximum machine accuracy attainable in double-precision mode. A space grid with 80 subintervals was used to allow for the rapid transition from the transport characteristics of thin DLs to the characteristics of thick descending prebend segments. In the numerical method, a model loop of Henle reaches to the right endpoint of each of the subinter-

Table 3. *Boundary conditions at corticomedullary boundary*

Variable	DL	CD	Ref
C, mM	130	130	41
F_V , nl/min	5.53	0.500*	5, 80

C, Cl^- concentration; F_V , fluid flow rate. *Per looped nephron.

vals; thus 80 loops of Henle are represented in the model calculations. Test calculations with 160, 320, and 640 subintervals yielded steady-state CD effluent osmolalities that are converging at a rate better than second order to a value that is $\sim 0.54\%$ less than the base-case value obtained with 80 subintervals. Test calculations demonstrated second-order spatial convergence for net mass and water flow through the simulated medullary cone.

Relative efficiency and relative concentrating effect. Some of the parameter studies reported in RESULTS make use of a measure of relative efficiency, which we now explain. The concentrating mechanism depends on several processes that require the sustained consumption of metabolic energy. These processes include the general maintenance of renal tissues, the pumping of fluid through the renal vasculature and tubules, the active transport of NaCl from proximal and distal tubules, and the active transport of NaCl from thick limbs. Of these processes, the one most intimately connected with the concentrating mechanism is NaCl active transport from thick limbs of Henle. The rate of transport is directly proportional to the energy consumed, owing to the nature of the $\text{Na}^+\text{-K}^+\text{-ATPase}$ pump. Thus, to assess the efficiency of the concentrating effect, one may compare the net urine concentrating effect with the total rate of active transport from all thick limbs of Henle. Because fluid is delivered to the avian kidney at plasma osmolality, the net urine concentrating effect is proportional to the U/P osmolality ratio minus 1. To obtain a measure of efficiency, we divided the net concentrating effect by the total rate of active transport. To provide a unitless measure of efficiency that is relative to that of the base case, we normalized that quotient by the analogous quotient corresponding to the efficiency of the base case. Thus we defined the relative efficiency by

$$\text{relative efficiency} = \frac{[(\text{U/P})(v) - 1]/\text{TAT}(v)}{[(\text{U/P})_b - 1]/\text{TAT}_b} \quad (1)$$

where $(\text{U/P})(v)$ is the simulated urine osmolality divided by the plasma osmolality when the model is evaluated for a value v of a stipulated parameter (all other parameters are set to their base-case values), and where $(\text{U/P})_b$ is the base-case U/P osmolality ratio. The total rate of active Cl^- transport (which is entirely from thick DLs and ALs) is $\text{TAT}(v)$; the corresponding base-case value is TAT_b . The definition is formulated so that the “relative efficiency” is 1 when a stipulated parameter v takes on the base-case value. A precise characterization of TAT is provided in the APPENDIX.

A second unitless quantity used in RESULTS is the relative concentrating effect, which is the net urine-concentrating effect for a particular parameter value (i.e., the U/P osmolality ratio $- 1$) normalized by the base-case net concentrating effect, i.e.

$$\text{relative concentrating effect} = \frac{[(\text{U/P})(v) - 1]}{[(\text{U/P})_b - 1]} \times 100\% \quad (2)$$

RESULTS

Base case. Fundamental base-case quantities obtained from the model are summarized in Table 4. These values include osmolality ratios at the cone tip and flow and absorption data for the longest loop, the aggregate loops, the CD system, and the whole medullary cone. Fundamental spatially distributed base-case model results are represented in Fig. 3 and Fig. 4, B–D.

Base-case tubular fluid-to-plasma (TF/P) osmolality ratios along the medullary cone are shown in Fig. 3. The curves labeled “DL” and “AL” correspond to the longest DL and the longest AL, respectively. The osmolality of intratubular fluid in the terminal, thick part of the DL and in the AL is progressively reduced along the flow direction by the active transport of NaCl. As a result, the AL fluid that returns to the cone base is significantly hyposmotic with respect to blood plasma (~ 218 mosmol/kg H_2O) compared with a plasma osmolality of 239 mosmol/kg H_2O . The NaCl

Table 4. Base-case simulation values

Osmolality ratios at cone tip	
U/P*	2.255
TF/P, bend of longest loop of Henle	2.257
TF/P, CC	2.715
Longest Loop of Henle	
Flow into DL at cone base†	5.530 nl/min
Flow at loop bend	4.424 nl/min
Flow out of AL at cone base	3.830 nl/min
Net DL absorption rate, H_2O	1.106 nl/min
Net AL absorption rate, H_2O	0.594 nl/min
Cl^- advection into DL at cone base†	718.9 pmol/min
Cl^- advection at loop bend	1,298 pmol/min
Cl^- advection out of AL at cone base	427.8 pmol/min
Net DL absorption rate, Cl^-	-579.4 pmol/min
Net AL absorption rate, Cl^-	870.5 pmol/min
Aggregate Loops of Henle‡	
Flow into DLs at cone base†	5.530 nl/min
Flow out of ALs at cone base	5.049 nl/min
Net absorption rate, H_2O	0.4818 nl/min
Cl^- advection into DL at cone base†	718.9 pmol/min
Cl^- advection out of AL at cone base	599.5 pmol/min
Net absorption rate, Cl^-	119.5 pmol/min
CD System‡	
Flow at cone base†	0.500 nl/min
Urine flow	0.2545 nl/min
Net absorption rate, H_2O	0.2455 nl/min
Cl^- advection at cone base†	65.00 pmol/min
Urine Cl^- advection	74.61 pmol/min
Net absorption rate, Cl^-	-9.615 pmol/min
Medullary Cone‡	
Net absorption rate,§ H_2O	0.7274 nl/min
Net absorption rate,§ Cl^-	110.0 pmol/min
Active absorption rate, Cl^-	353.4 pmol/min

CC, central core. *Avian urine undergoes substantial postrenal alteration before being excreted (31). †Boundary condition, stipulated a priori. ‡Scaled per looped nephron. §From all tubules, including CDs.

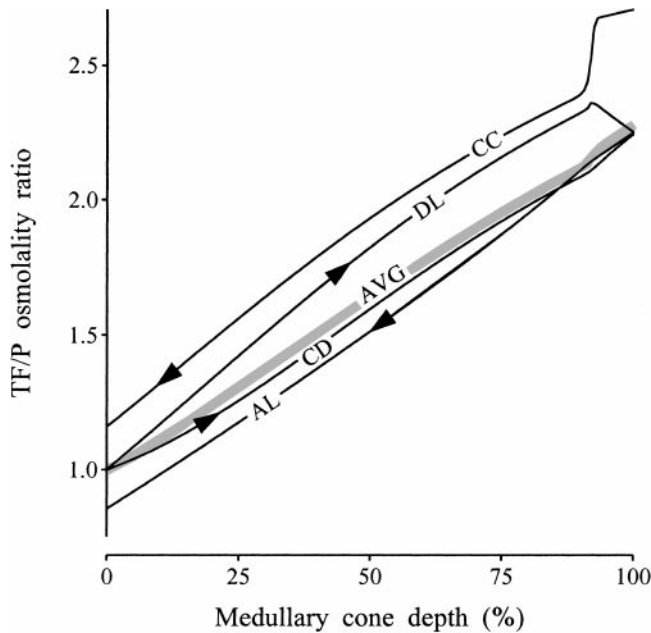


Fig. 3. Profiles of base-case tubular fluid-to-plasma (TF/P) osmolality ratios in longest loop of Henle (DL and AL), collecting duct (CD), and central core (CC). Arrows indicate flow directions. Gray line (AVG) gives average of osmolality in all represented structures, weighted according to cross-sectional area. The CC profile gives osmolality of the accumulated net absorbed fluid, which flows from medullary cone tip to cone base. The CC profile increases rapidly to a high plateau near cone tip, because only thick limbs of Henle are present in deepest 255 μm of cone. In general, osmolality profiles appear to increase linearly, but a closer examination reveals that, with the exception of the AL, profiles tend to be concave down.

absorbed from the thick segments raises the osmolalities in the DL, the CD system, and the CC. The CC exhibits a large rise in osmolality in the 0.25 mm nearest the cone tip, because the NaCl absorbed from the near-bend thick segments of the longest loops of Henle is not in apposition with any thin DL segments.

The curve labeled "AVG" in Fig. 3 shows the average TF/P osmolality ratio in all structures represented in the model, weighted according to the cross-sectional areas of all structures (this curve is comparable to values that could be obtained from a tissue-slice experiment). To obtain the weighted average, the TF/P osmolality ratio in each tubule, at each medullary level, was multiplied by its cross-sectional area, and all such products were summed together to obtain a value S_M . To obtain the appropriate weighting, the summands corresponding to loops of Henle were weighted according to the fraction of loops reaching each level, and, for the purposes of this calculation, the CC was counted as a tubule. The sum S_M , with units of area, was then divided by the total cross-sectional area of all tubules, at the corresponding level, to obtain the values labeled by AVG. Because the CD is the dominant structure near the cone tip in terms of cross-sectional area, the average osmolality near the cone tip closely approximates CD osmolality.

In a CC model, the osmolality in the CD is influenced directly only by the CC osmolality. The osmolality of

the CD flow tracks the axial increase in CC osmolality, but because of the base-case CD osmotic water permeability of 115 $\mu\text{m/s}$ [which is low relative to the value of 445 $\mu\text{m/s}$ measured in rabbit CD (28, 61)] and the magnitude of the CD flow, CD osmolality at each medullary level lags below that of the CC.

To a first approximation, the TF/P osmolality ratios shown in Fig. 3 increase linearly as a function of cone depth, but comparison with a straight-edge will show that the curves tend to be concave down, except for the AL. This concavity suggests that the load presented by flow in the CD becomes less well matched by the concentrating capacity of the loops of Henle as medullary depth increases. The concave-downward property is consistent with tissue-slice studies reported in Fig. 7 of Ref. 16 (see DISCUSSION).

Figure 4, B–D, exhibits level curves of loop of Henle concentration, water flow, and Cl^- advection. (Figure 4A, described in MATHEMATICAL MODEL, represents loop of Henle diameters used in the model formulation.) The results exhibited in Fig. 4 are generally consistent with our expectations. The level curves of Cl^- concentration in Fig. 4B indicate that DLs, at each level, are in near osmotic equilibrium, which is consistent with their high permeability to NaCl. The curves for AL concentration (Fig. 4B) also indicate similar osmolalities at each level, but there is less consistency at each level. The reduced consistency can be reasonably attributed to the varying diameters, as a function of cone depth (because diameter is proportional to available transport area and inversely proportional to flow speed), and to the more complete saturation of active transport at high than at low concentrations. Nonetheless, at each level the concentrations are sufficiently similar among all limbs of Henle that Fig. 4B serves as an illustration of a key aspect of the theory of countercurrent multiplication: at each fixed medullary level the concentrations (and, hence, in this case, osmolalities) of tubular fluid vary little from tubule to tubule relative to the difference generated along the flow axis from the cone base to the cone tip.

The level curves of water flow, exhibited in Fig. 4C, indicate a greater water loss from DLs than from ALs, consistent with the higher water permeability of DLs (552 vs. 57.2 $\mu\text{m/s}$ for ALs). In the diagonal strip corresponding to the PBE (the strip between the gray dashed line and the gray line) and in the region corresponding to the ALs, the level curves tend to be more nearly parallel to the flow direction, which indicates an approximation to constant intratubular flow.

The level curves of Cl^- advection (Fig. 4D) illustrate Cl^- (and, hence, NaCl) cycling from thick limbs to thin DLs. By comparison with Fig. 4C, one can determine that the fluid in the DLs is principally concentrated by the addition of Cl^- . Indeed, numerical results from the model indicate that, in the thin portion of the DL of the longest loop, 79.9% of the increase in osmolality arises from solute addition, whereas only 20.1% arises from water absorption. Advection of Cl^- in the ALs of longer loops is more reduced at each level than advection in shorter loops. This difference (similar to the case of Cl^-

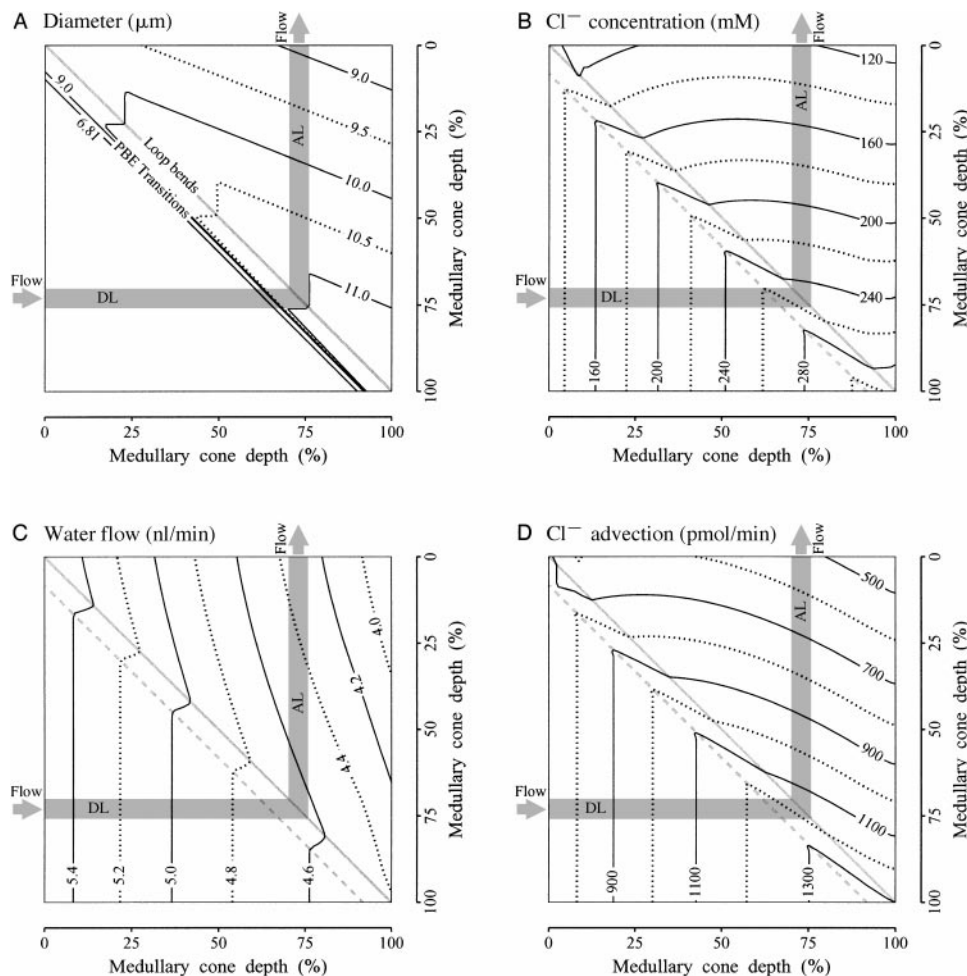


Fig. 4. Level curves of quantities associated with loop of Henle distribution. Left vertical axes, DL values at cone base; top horizontal axes, AL values at cone base; bottom horizontal axes, longest DL; right vertical axes, longest AL; diagonal line from *top left to bottom right* (gray line), loop bends. In lower left triangles, DL length increases along horizontal axis, from left to right; in upper right triangles, AL length increases along vertical axis, from top to bottom. Wide gray lines suggest a representative loop of Henle that reaches $\sim 75\%$ of the distance into the medullary cone; arrows indicate normal flow direction of intratubular fluid. Gray dashed lines in *B–D* correspond to site of PBE transitions from thin to thick DLs. Variables in *A–D* are constant along each level curve and take on the value labeled on the curve. Except in *A*, level curves were constructed to give equal increments of represented quantity. The level curves permit the value of each quantity to be represented as a function of loop length and medullary depth. *A*: inner diameters of tubules based on measurements of Casotti et al. (11). Thin limbs, i.e., limbs before PBE transitions, are of nearly constant diameter of $\sim 6.81 \mu\text{m}$, corresponding to lower triangular region having no curves. *B*: base-case Cl^- concentration. Concentrations within thin DLs are nearly uniform at each medullary level; concentrations within thick limbs also tend to be uniform at each medullary level, but less so than in thin limbs. *C*: base-case intratubular water flow rate. Some water is absorbed from thin DLs, which are somewhat water permeable; little water is absorbed from ALs, which have much lower water permeability. *D*: base-case Cl^- advection rate. Substantial Cl^- (and, hence, NaCl) enters thin DLs, while Cl^- advection rate is nearly uniform in DLs at each fixed medullary level. Different amounts of Cl^- are absorbed from thick limbs as a function of loop length, leading to differing thick limb Cl^- advection rates at each fixed medullary level.

concentrations) arises because the reduced flow speed and increased surface area in longer ALs result in greater transepithelial active transport than in shorter limbs.

In summary, the results from the base case indicate that 1) urine is concentrated by means of a countercurrent multiplier that relies on active NaCl transport from ALs to generate the single effect, 2) this countercurrent multiplier system employs NaCl cycling from ALs to DLs, 3) fluid in DLs is principally concentrated

by NaCl addition, 4) the NaCl concentrations (and osmolalities) within all DLs will tend to be nearly equal to each other at each level, and the analogous result is predicted for ALs, and 5) the osmolality profiles in the tubules of the medulla tend generally to be linear, with a slight concavity, oriented down. These results are consistent with the countercurrent hypothesis advanced by Skadhauge and Schmidt-Nielsen (66) and the NaCl cycling hypothesis advanced by Nishimura et al. (51).

Parameter studies. Extensive studies were conducted to determine the sensitivity of the results to changes in base-case parameter values. In most studies, a single parameter was varied systematically while all other parameters retained their base-case values. In these studies, the stipulated parameter was incrementally increased and the corresponding steady-state solution was computed. The size of the increment was determined empirically to yield smooth curves. However, some studies involved special cases in which two parameters were simultaneously changed from base-case values. In the results given below, those studies will be clearly distinguished from the single-parameter studies.

Permeability to water and Cl^- . Figure 5 exhibits results obtained by varying the osmotic water permeability and the Cl^- permeability of the represented tubules. Each curve represents a numerical experiment in which only one parameter was changed in one tubule; all other parameters remained at base-case values. In Fig. 5 and in similar subsequent figures, the gray horizontal bar indicates the base-case value of the quantity represented as the ordinate. Each open circle corresponds to a base-case value of a parameter that is varied along the interval of abscissa values. A wide black curve segment, where present, corresponds to the standard deviation (or, alternatively, range) of a measured experimental value as reported in the literature.

The results in Fig. 5A indicate that concentrating capability is nearly independent of DL osmotic water permeability. However, a low AL permeability and a sufficiently high CD permeability are essential for a significant concentrating effect. The results in Fig. 5B1 indicate that concentrating capability is nearly independent of CD Cl^- permeability. In cases in which CD Cl^- permeability exceeded the base-case permeability, the osmolality of CD fluid more closely approximated CC osmolality than in the base case, but DL and CC osmolalities were reduced relative to the base case. However, for high Cl^- permeability, CD equilibration was mostly by Cl^- entry, so that a much larger amount of concentrated urine was produced per looped nephron, viz., 0.488 nl/min, which is only slightly diminished from the base-case CD inflow of 0.500 nl/min and is 191% of the base-case urine flow of 0.255 nl/min. This result suggests that the modulation of CD Cl^- permeability *in vivo* might provide a mechanism for the regulation of the rates of electrolyte and water excretion that would not compromise concentrating capability.

The results in Fig. 5B2 indicate that concentrating capability is not much affected by variation in DL Cl^- permeability, provided that its value exceeds $\sim 50 \times 10^{-5}$ cm/s. Even when DL Cl^- permeability is reduced to zero, the U/P osmolality ratio is reduced only to 2.02 from the base-case value of 2.26. This indicates that NaCl cycling from AL to DL is not required for the system to generate a significant concentrating effect. Results in Fig. 5B2 indicate that even small increases in AL Cl^- permeability substantially decrease concentrating capability. The system is sensitive to AL Cl^-

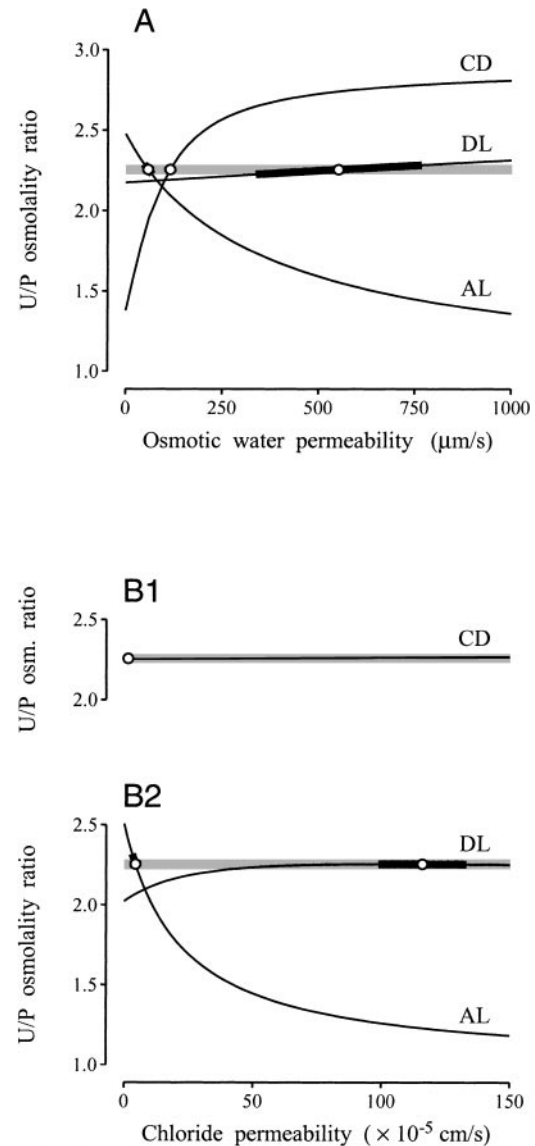


Fig. 5. Water and Cl^- permeability sensitivity studies. Horizontal gray bars, base-case urine-to-plasma (U/P) osmolality ratio, ~ 2.26 ; curves, model U/P osmolality ratios obtained by varying permeabilities in indicated tubule types; \circ , base value of each parameter; wide black curve segments, experimental range for varied parameter, if known. A: sensitivity of U/P osmolality ratio to osmotic water permeability of DL, AL, and CD. U/P osmolality ratio is nearly insensitive to DL permeability, sensitive to AL permeability, and very sensitive to CD permeability for values below $\sim 200 \mu\text{m/s}$. B1: U/P osmolality ratio is insensitive to permeability of CD to Cl^- (but urine flow can be significantly affected; see text). B2: sensitivity of U/P osmolality ratio to AL and DL Cl^- permeability. U/P osmolality ratio is insensitive to DL permeability for values above $\sim 50 \times 10^{-5}$ cm/s, but U/P ratio is sensitive to increasing AL permeability, which diminishes net absorption of Cl^- from ALs.

permeability because Cl^- backleak directly opposes the Cl^- active transport (the source of the single effect) that is required for countercurrent multiplication.

Two cases were examined in which two parameters were simultaneously changed from the base case. In the first, water and Cl^- permeability were set to zero for all thin segments of DLs. The resulting U/P osmo-

lality ratio was 2.01, a decrease in relative concentrating effect of 20% compared with the base case (see Eq. 2 for definition of relative concentrating effect). However, in this case, the TF/P osmolality ratio of fluid entering the cortex via the CC was 1.76 (for the base case it was 1.16), whereas the TF/P osmolality ratio of flow-weighted AL fluid entering the cortex was 0.820 (for the base case it was 0.913). Moreover, 21% more fluid was absorbed from thick limbs than had been absorbed from thin and thick limbs of Henle combined in the base case, owing to the higher osmolality in the CC near the medullary cone base. The increased solute and fluid load presented to the vasculature by absorption from loops of Henle would likely have reduced the effectiveness of vascular countercurrent exchange, if the vasculature had been explicitly represented in our model. These hypothetical results for thin DLs lacking water and NaCl transport underline the importance of the likely normal role of these tubules in supporting a countercurrent multiplier system with small transverse osmotic gradients between the lumens of the different types of tubules.

In the second case, water and Cl^- permeability were simultaneously set to zero for the entire CD system. In this case, there was essentially no (useful) load on the concentrating mechanism. T/P osmolality ratios increased to 3.33 and 4.25 in the bend of the longest loop of Henle and in the CC at the cone tip, respectively. These values and the results reported below in Fig. 7A indicate that the maximum theoretical U/P osmolality ratio for a nearly vanishing CD flow ranges from ~ 3 to 4.

Rate of active Cl^- transport from thick limbs. The curve in Fig. 6A indicates, as expected, that concentrating capability increases as the maximum rate of active Cl^- transport from thick limbs (V_{\max}) is increased. Moreover, the curve is concave upward, which indicates that osmolality increases more rapidly as the transport rate increases. Since Fig. 6B shows that total active transport from all thick limbs increases nearly linearly with increasing V_{\max} , the increasing sensitivity of concentrating capability as V_{\max} increases cannot be attributed to incomplete saturation of the (assumed) Michaelis-Menten transport. Rather, the explanation may be found in the expressions derived for simple CC models, which show that the U/P osmolality ratio tends to increase nonlinearly with increased absorption from thick limbs (44, 70). Consistent with the effect noted in Fig. 6A, the relative efficiency reported in Fig. 6C shows that the efficiency of concentrating capability increases with increasing V_{\max} . (The definition for relative efficiency was given by Eq. 1.)

An analogous study for the Michaelis constant (K_m) (data not shown) resulted in monotone and parallel decreases in the U/P osmolality ratio, total active transport, and relative efficiency as the K_m was increased from 0 to 600 mM. The decreases were more rapid for smaller values of K_m (and near the base-case value of 40 mM) than for larger values. This pattern, which is roughly inverse to that of the study for V_{\max} ,

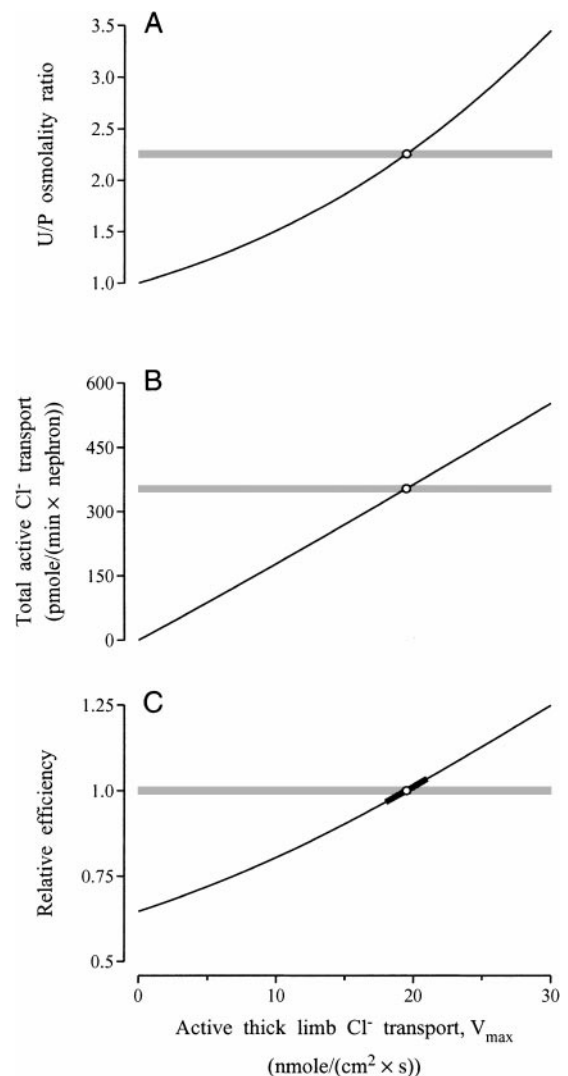


Fig. 6. Model sensitivity to maximum active transport rate from thick limbs (V_{\max}). A: U/P osmolality ratio as a function of V_{\max} for active Cl^- transport from thick limbs. Gray horizontal bar, base-case osmolality; \circ , base-case value for V_{\max} . U/P osmolality ratio increases with increasing active transport rate, as expected; however, the rate of increase of U/P osmolality ratio also increases with increasing transport rate. B: total active transport rate across all thick limbs as a function of V_{\max} expressed per looped nephron. Gray horizontal bar, base-case total active transport rate from all thick limbs; \circ , base-case value for V_{\max} . Nearly linear increase indicates that total transport is nearly proportional to V_{\max} . C: relative efficiency as a function of V_{\max} . Gray horizontal bar, base-case efficiency, which is 1 by the measure of efficiency used; \circ , base-case value for V_{\max} . Wide black curve segment corresponds to experimental range of V_{\max} . The relative efficiency of the concentrating mechanism increases with increasing values of V_{\max} .

is explained by the reciprocal effects of K_m and V_{\max} (see Eq. A4 in APPENDIX).

DL and CD input flow. The inflow rates into the DLs and the CD system at the corticomedullary boundary are important parameters whose values have been inferred from other measurements of related quantities (see *Model parameters*). The effects of varying these parameters are shown in Fig. 7. In Fig. 7A, CD input flow was increased far beyond its base-case value (per

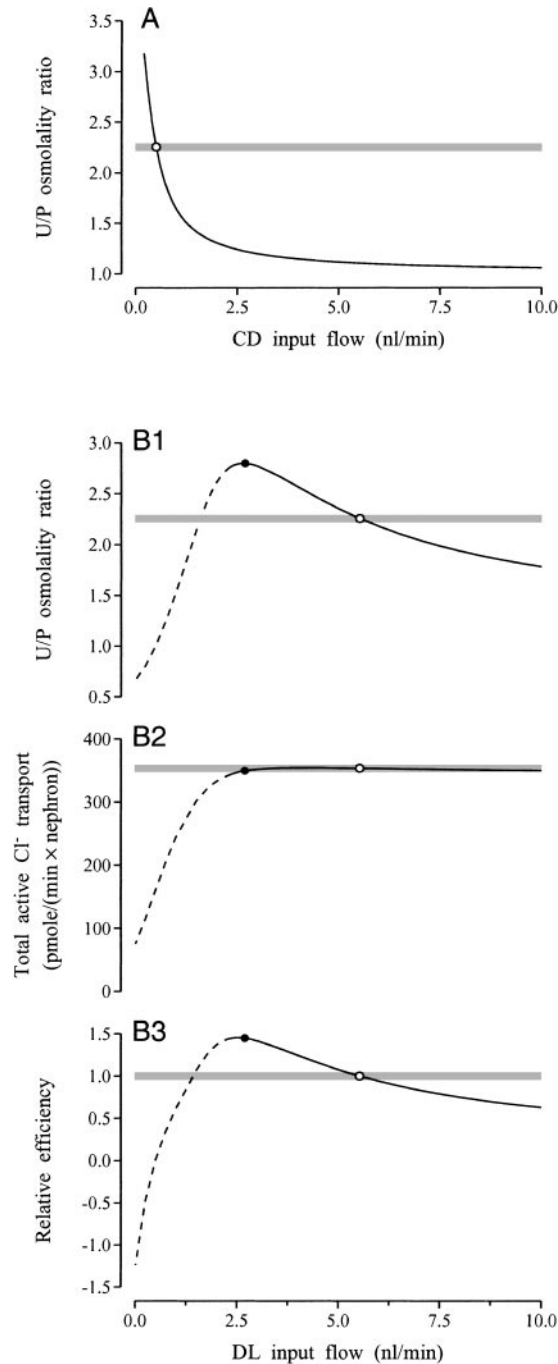


Fig. 7. A: sensitivity of U/P osmolality ratio to CD input flow at corticomedullary boundary. Gray horizontal bar, base-case U/P osmolality ratio; \circ , base-case input flow of 0.5 nl/min. Osmolality ratio rapidly declines for values near base-case input flow. B1–B3: model study of sensitivity to DL input flow at corticomedullary boundary. Gray horizontal bars, base-case values. For flow less than ~ 2.2 nl/min, intratubular flow direction reverses at sites along some of the loops of Henle, because transepithelial flux from loops exceeds the input flow (dashed lines). \bullet , Maximum U/P osmolality ratio of 2.8 and corresponding total active Cl⁻ transport and relative efficiency, at input flow of 2.7 nl/min; \circ , U/P osmolality ratio, total transport, and relative efficiency at base-case input flow of 5.53 nl/min. As input flow increases through the interval containing the base-case value, osmolality decreases with increasing flow (B1), active transport is not much affected (B2), and relative efficiency decreases (B3).

nephron) of 0.500 nl/min, which resulted in a marked decrease in the U/P osmolality ratio. Indeed, a doubling of the base-case value to 1.00 nl/min decreased the U/P osmolality ratio from the base-case value of 2.26 to 1.64, which is a 49% decrease in relative concentrating effect.

The sensitivity to DL input flow is shown in Fig. 7, B1–B3. The dashed lines indicate an interval in which input flow below the base-case flow of 5.53 nl/min results in intratubular flow reversal in at least some portions of some loops of Henle. It is doubtful that such an effect could arise in vivo, unless tubuloglomerular feedback were disabled. Therefore, model results corresponding to the dashed lines should probably be disregarded, except as indicating the need for adequate NaCl from DL inflow to drive the concentrating mechanism and the important role of regulatory processes that were not included in the model. The filled circle in Fig. 7B1 indicates the maximum U/P osmolality ratio, 2.80, for the range of input flows examined. Corresponding filled circles have been placed on Fig. 7, B2 and B3. The open circle indicates the base-case values. Over most of the valid range of the applicability of this study, the U/P osmolality ratio is decreasing, reaching a value of 1.78 at a DL input flow of 10 nl/min. The rate of total active Cl⁻ transport is nearly unaffected, which suggests compensation for decreased Cl⁻ concentrations in the Michaelis-Menten transport term (in Eq. A4), arising from the diluting effects of higher flow, by the increased availability of Cl⁻, which is carried into DLs in amounts proportional to DL input flow at the cone base. Because total active transport is nearly unaffected, the decrease in U/P osmolality ratio may be attributed to the increasing osmotic load presented to the concentrating mechanism by increased flow in thin DLs. Also, because the total active transport is nearly unaffected, relative efficiency follows the same pattern as the decrease in osmolality ratio.

Rate of active Cl⁻ transport from CDs. For the base case, we assumed that Cl⁻ transport from the CD system is negligible, and we therefore took V_{\max} for the CD system to be zero. To assess parameter sensitivity and to determine whether this is a reasonable assumption, we conducted studies where V_{\max} for the CD ranged from 0 to 5 nmol·cm⁻²·s⁻¹. Because a sufficiently large active transport rate can result in significantly increased water absorption from the CD system accompanied by unrealistically low urine flow, we also considered the effects of increasing CD input flow at the cone base while simultaneously varying the V_{\max} for the CD system.

The results of these studies are summarized in Table 5. The base-case CD input flow of 0.500 nl/min per looped nephron is our estimate based on measured urine flow of 0.27 nl/min per looped nephron and the assumption that CD fluid is concentrated principally by water absorption from the CD (see *Model parameters*). For base-case CD input flow, an increase of V_{\max} to 1 nmol·cm⁻²·s⁻¹ results in a U/P osmolality ratio that is little changed and a urine flow of 0.213 nl/min per looped nephron, a value that remains consistent

Table 5. Effects on urine composition of active Cl^- absorption from the CD system

V_{\max}	CD Input Flow per Looped Nephron								
	0.500 nl/min			0.750 nl/min			1.00 nl/min		
	U/P	\dot{U}	\dot{S}	U/P	\dot{U}	\dot{S}	U/P	\dot{U}	\dot{S}
0	2.26	0.255	74.6	1.86	0.451	109	1.64	0.671	143
1	2.27	0.213	62.8	1.83	0.412	97.5	1.60	0.633	131
3	2.36	0.129	39.6	1.74	0.329	74.6	1.49	0.557	108
5	2.72	0.0479	16.9	1.64	0.247	52.5	1.37	0.482	86.1

V_{\max} , maximum active transport rate of Cl^- from CD ($\text{nmol}\cdot\text{cm}^{-2}\cdot\text{s}^{-1}$); U/P, urine-to-plasma osmolality ratio; \dot{U} , urine flow per looped nephron (nl/min); \dot{S} , urine Cl^- advection per looped nephron (pmol/min).

with the experimental value, 0.27 nl/min. However, as V_{\max} is increased to $5 \text{ nmol}\cdot\text{cm}^{-2}\cdot\text{s}^{-1}$, urine flow falls significantly to 0.0479 nl/min, while the U/P osmolality ratio increases to 2.72, a value that exceeds the concentrating capability of most birds.

For a CD input flow of 0.750 nl/min per looped nephron in Table 5, a V_{\max} of $5 \text{ nmol}\cdot\text{cm}^{-2}\cdot\text{s}^{-1}$ produces a U/P osmolality ratio and urine flow rate that are most consistent with experiments: 1.64 and 0.247 nl/min, respectively. However, in the case of this CD input flow, there is the paradoxical result that as solute absorption from the CD increases, the U/P osmolality ratio decreases well below the base-case value of 2.26, even though for a V_{\max} of $5 \text{ nmol}\cdot\text{cm}^{-2}\cdot\text{s}^{-1}$ the central core TF/P osmolality ratio is 2.44 at the cone tip. The vigorous active Cl^- transport tends to dilute CD contents (relative to flow in the CC and loops of Henle), because the base-case osmotic water permeability is not large enough to allow near-osmotic equilibration of CD fluid with CC fluid when the input CD flow and Cl^- absorption from that flow are sufficiently large. This disparity is inconsistent with a key principle of countercurrent multiplication: for efficient and effective operation, at each level the flows in all tubules should vary little in osmotic pressure.

For a CD input flow of 1.00 nl/min per looped nephron (as in the case of 0.750 nl/min) in Table 5, the CD does not attain near-osmotic equilibration with the CC, which has a cone tip TF/P osmolality ratio of 2.27 for a V_{\max} of $5 \text{ nmol}\cdot\text{cm}^{-2}\cdot\text{s}^{-1}$. Moreover, urine flows remain superphysiological throughout the examined range of V_{\max} . Thus, for a CD inflow of 1.00 nl/min, the concentrating mechanism is simply overwhelmed.

Because of its general consistency with urine flow, urine osmolality, measurements of CD osmotic water permeability, and countercurrent multiplier theory, a reasonable conclusion from the results in Table 5 is that the most likely parameter combination is a base-case CD input flow rate of $\sim 0.5 \text{ nl/min}$ per looped nephron with a V_{\max} for CD Cl^- transport that is not significantly larger than $1 \text{ nmol}\cdot\text{cm}^{-2}\cdot\text{s}^{-1}$.

Cone length. The effect of cone length on concentrating capability is illustrated in Fig. 8. In these studies, the length of the PBEs was unchanged; the added length was given to thin DLs and to ALs. Thus, when cone length decreased below 0.255 mm, loops of Henle consisted entirely of thick limbs. As shown in Fig. 8A, increasing cone length to 12 mm increased the U/P

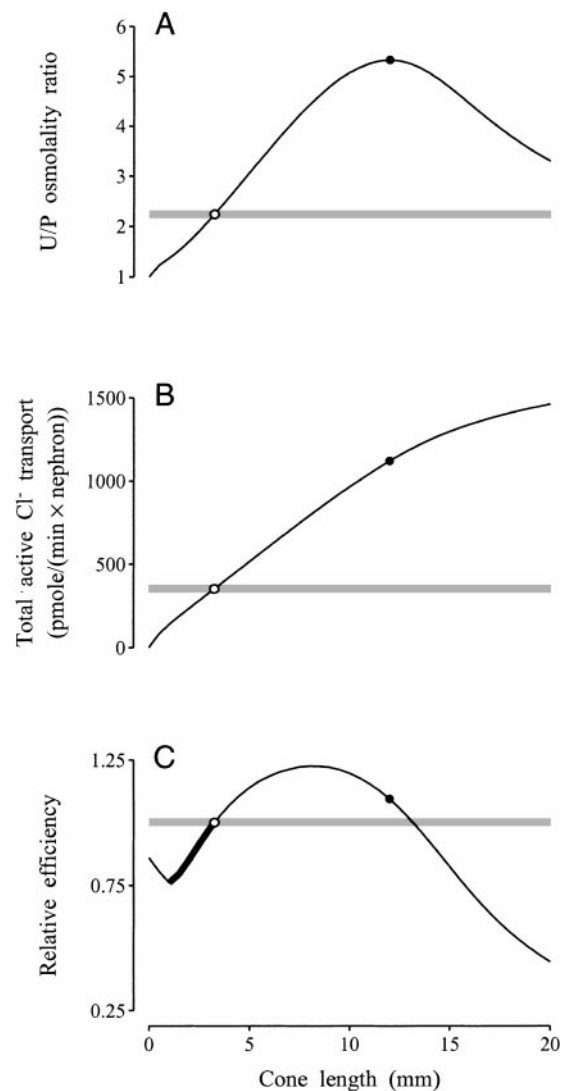


Fig. 8. Model sensitivity to cone length. A: U/P osmolality ratio as a function of cone length increases to a maximum value of 5.3 (●) at length of 12 mm and then decreases. Gray horizontal bar, base-case U/P osmolality ratio; ○, base-case cone length, 3.25 mm. B: total active Cl^- transport increases monotonically as a function of loop length. Gray horizontal bar, base-case total transport. C: relative efficiency as a function of loop length. Gray horizontal bar, base-case efficiency of 1; wide black curve segment, experimental range for cone length. Some efficiency is gained by increasing cone length beyond experimental values, but sufficiently long cone length results in efficiency being substantially reduced below base-case efficiency.

osmolality ratio by 344% over the base case, but additional increases in length led to concentrating capabilities that were substantially below the maximum achievable osmolality. A potential explanation for the decline in concentrating capability for sufficiently long cones is suggested by Fig. 8B, which shows that the total active Cl^- transport rate increases more slowly for sufficiently long cones, presumably because only limited Cl^- is available to be pumped from thick limbs.

Although the concentrating capability can be dramatically increased by lengthening the cone, the relative efficiency, shown in Fig. 8C, increases only to a maximum of $\sim 123\%$ at cone length of 8 mm and then decreases as cone length increases further. Thus a gain in efficiency of only 23% is obtained by the 246% increase in cone length from 3.25 to 8 mm.

Experimentally measured cone lengths in Gambel's quail correspond to the thick black curve segment in Fig. 8C. As cone length ranges from 1.0 to 3.25 mm, the U/P osmolality ratios increase from 1.37 to 2.26. These values are consistent with maximum U/P osmolality ratios found in birds, ratios that seldom exceed 2.0–2.5 (4, 20). The decrease in relative efficiency to a local minimum of ~ 0.76 near a length of 1 mm (Fig. 8C) may be attributable to the appearance of thin descending segments, which, at first, may reduce the concentrating capacity afforded by the presence of thick limbs, which are the only type of limbs present in the model when medullary cone length is < 0.255 mm.

Length of PBE. Results collected in Fig. 9 indicate that concentrating capacity is sensitive to the length of the PBE, i.e., to the length of the thick, terminal portion of the DL, which is assumed to have the same transport properties as the AL. The relative location of the PBE is illustrated in Fig. 9A. The dependence of concentrating capability on the length of the PBE is shown in Fig. 9B1. As the prebend length increases from zero to its base-case value of 255 μm , the U/P osmolality ratio increases from 1.74 to 2.26 (open circle), which corresponds to a 70% increase in relative concentrating effect. As the prebend length increases further to 905 μm (filled circle), the net concentrating effect increases to 266% of the no-PBE case.

Additional increases in PBE length, however, result in decreasing concentrating capacity. Examination of level curves for this case, analogous to those in Fig. 4, indicates that the decrease can be attributed to high absorption rates at early sites along DLs, reduced absorption at sites near loop bends, enhanced water absorption from loops of Henle (owing to gradients arising from enhanced tubular dilution), and limits in the amount of Cl^- that can be absorbed. Indeed, Fig. 9B2 shows that increasing PBE length beyond ~ 1 mm results in little additional total Cl^- transport. The amount of Cl^- that can be transported by a loop of Henle depends principally on the amount of NaCl advected into its thick segments from the thin DL. A lengthened PBE reduces the length of the thin DL segment available for diffusive Cl^- entry. Results in Fig. 9B3 show that the relative efficiency decreases substantially for PBE lengths that exceed the mea-

sured range (the measured range is indicated by the thick black curve segment).

Loop distribution. Figure 10A shows curves for the fraction of loops of Henle as a function of percentage of medullary cone depth. The gray exponential curve corresponds to our base case and closely follows the fractional distribution measured in a particular cone (same cone as represented in Fig. 2). The other curves correspond to other rates of exponential decrease; they are labeled according to the fraction of loops reaching to (and turning at) the cone tip. Thus, in the base case, ~ 4 of 100 of the loops reach to the cone tip.

Figure 10, B1–B3, illustrates the result of parameter studies in which osmolality ratios and rates of total active transport were computed for exponential curves that corresponded to a particular fraction of loops reaching the cone tip. As that fraction increased from near zero, the U/P osmolality ratio increased rapidly, to a maximum value of 2.44. That increase arises because, in the deepest part of the cone, the increasing fractions of loops provide increasing concentrating capacity to the remaining fluid flowing in the remaining CDs. If there are too few loops, then the fluid in the CDs presents a load that cannot be much affected by those loops.

However, as the fraction of loops reaching the cone tip increased further, the osmolality ratio decreased gradually. The decrease may be understood as follows. The osmotic load presented to the concentrating mechanism comes not only from CD flow, but also from flow in thin DLs, which (in the model) is concentrated principally by Cl^- entry. As more of the loops reach further in the cone, DL flow becomes the principal load on the concentrating mechanism and CD flow becomes an increasingly less significant factor. Moreover, there is less apposition of PBEs with thin DLs (and no apposition when all loops reach the cone tip). So the opportunity for a cascade, in which bends at almost all levels concentrate thin DL fluid but are not part of the osmotic load at the bend level, is reduced (44).

Total active transport (Fig. 10B2) increases by 318% from the base case to the case where all loops reach the cone tip. The increase arises from the increase in the combined length of thick limb segments (mostly thick AL segments).

The relative efficiency (Fig. 10B3) is monotonically decreasing: it decreases rapidly near the base case but more slowly as the fraction of loops reaching the tip increases. Figure 10B3, combined with the results in Fig. 10, B1 and B2, makes a persuasive case that the exponentially decreasing loop distribution found in vivo is consistent with an energetically efficient concentrating mechanism.

DISCUSSION

Model assumptions and modeling methodology. The model used in this study is based on standard assumptions and numerical methods that have been used in studies of the mammalian urine concentrating mechanism (see references in Ref. 63). The CC assumption,

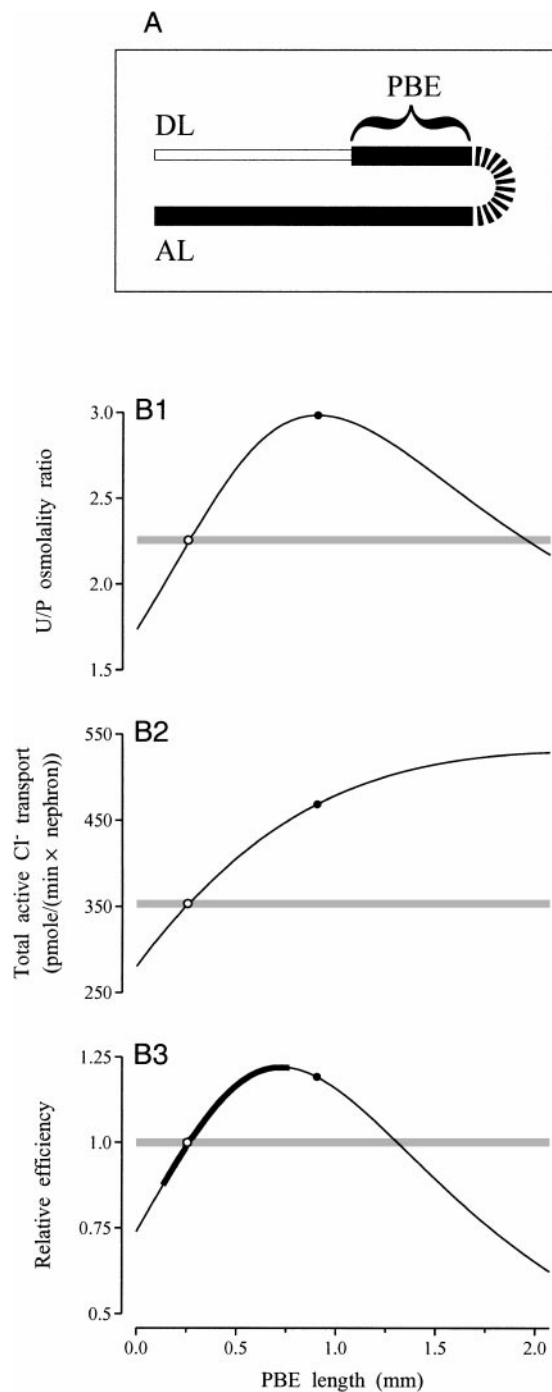


Fig. 9. Model sensitivity to length of PBE. *A*: schematic diagram showing loop of Henle with PBE. *B1*: U/P osmolality ratio as a function of PBE length increases to 2.98 (●) at PBE length 0.905 and then decreases. Gray horizontal bar, base-case osmolality; ○, base-case value of PBE length, 255 μm . As the PBE length increases from zero to the base-case value, the U/P osmolality ratio increases from 1.74 to 2.26, which corresponds to a 70% increase in relative concentrating capability. *B2*: total active Cl^- transport by all thick limbs increases monotonically as the total length of thick limb segments increases; however, the rate of increase of total transport decreases, presumably because progressively less Cl^- is available from solute cycling from thick limbs to thin DLs. Gray horizontal bar, base-case total transport; ○, base-case PBE length. *B3*: relative efficiency as a function of PBE length. Wide black curve segment corresponds to the experimental range of PBE length. As PBE length increases beyond experimental values, the decrease in U/P osmolality ratios (*B1*) results in a rapid decrease in relative efficiency.

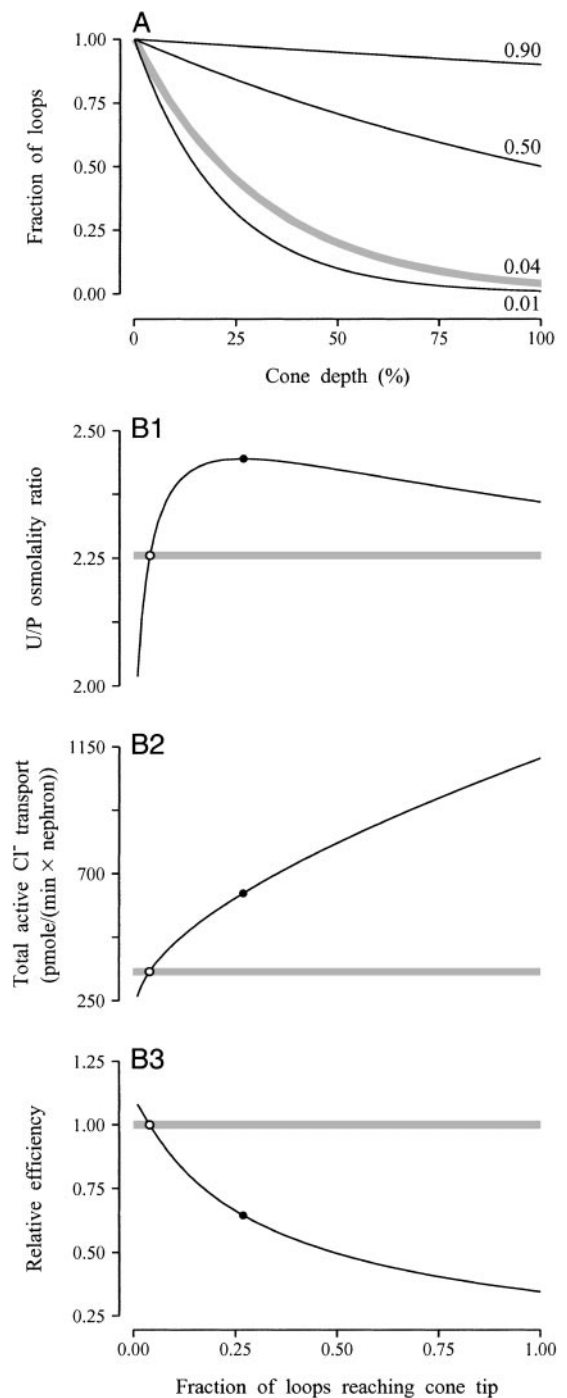


Fig. 10. Model sensitivity to loop distribution. *A*: fraction of loops of Henle as a function of cone depth for 4 different exponential decrease rates. Labels (0.01, 0.04, 0.5, and 0.9) correspond to fractions of loops reaching cone tip at those decrease rates. Gray curve (labeled 0.04) corresponds to the base case. *B1*: U/P osmolality ratio increased to a maximum of 2.44 (●) as the fraction of loops reaching the cone tip increased to 0.27. Gray horizontal bar, base-case osmolality ratio; ○, fraction of loops reaching cone tip in the base case, 0.04. *B2*: total active Cl^- transport as a function of fraction of loops reaching the cone tip increased monotonically, since the total length of thick segments increases as the fraction of loops reaching the cone tip increases. Gray horizontal bar, total active transport in the base case. *B3*: relative efficiency as a function of the fraction of loops reaching the cone tip. Efficiency declines, more rapidly for smaller fractions, as the fraction of loops reaching the cone tip increases to 1.

introduced by Stephenson (70) and employed in this model, merges the renal vasculature with the interstitial space into a single tubule (the CC) and thus has the advantage that an explicit representation of the medullary vasculature is not required. This formulation is reasonable, inasmuch as the transport properties of the avian medullary vasculature have not been investigated and the medullary vasculature of small mammals, such as the rat, has been found to be highly permeable to water and solutes (54–58). Theoretical and simulation studies (34, 71) indicate that the CC formulation provides good approximations to vascular countercurrent exchange if the vasa recta and associated capillary beds are sufficiently permeable to water and small solutes. Because the CC assumption is equivalent to assuming perfect countercurrent exchange by the vasculature, the CC assumption has the probable effect of slightly overestimating achievable urine osmolality.

In addition, we assume that DLs, ALs, and the CD system interact with each other on an equal footing via the CC. Therefore, aspects of three-dimensional structure involving preferential interactions among tubules are not represented in the model. Such preferential interactions may play a substantive role in some avian species, notably the *Passeriformes*, which have a highly organized medullary cone structure (31). However, there is much less anatomic basis for preferential interactions in the gallinaceous species (i.e., Gambel's quail and the Japanese quail) on which this study is based (31).

The model formulation used here employs a representation that approximates the effect of discrete loops reaching to all levels of the avian medullary cone. This representation, which has been used in a number of previous studies (42–47), permits the estimation of tubular variables all along a loop of Henle, reaching to any level in the cone, unlike representations that employ the shunting of fluid from a composite DL to a composite AL (78). Moreover, the discretely distributed loops allow the explicit representation of active NaCl absorption from thick prebend segments of loops of Henle. Model results indicate that prebend active absorption is a key feature in the avian concentrating mechanism.

Experiments indicate that in most mammals a mechanism localized in the inner medulla and involving urea plays a significant role in concentrating urine (17, 62). However, mathematical models that have incorporated measured transport properties of NaCl and urea have not exhibited a significant inner medullary concentrating effect (63). This discrepancy, which has promoted further experimental activity and the development of increasingly sophisticated mathematical models, has brought into question the adequacy of experimental and modeling methodologies.

In contrast to the mammalian concentrating mechanism, experimental evidence indicates that the avian mechanism depends entirely on active NaCl transport to provide the driving force for the single effect required for countercurrent multiplication (51, 66). This

simpler physiological context provides a good test case to assess the adequacy of modeling methodology. The model employed in this study, which uses experimentally determined anatomic structures and transport properties, predicts concentrating capacity that is consistent with measurements of maximum avian urine osmolalities. Therefore, because this study has used standard mathematical formulations and techniques similar to those used in recent studies of the mammalian concentrating mechanism (see references in Ref. 63), this study supports the adequacy of mathematical modeling methodology for representing the urine concentrating mechanism. It should be acknowledged, however, that model frameworks using time-independent flows and rigid tubules are not adequate to evaluate some hypothesized concentrating mechanisms, such as those involving peristalsis of the papilla (63).

Most of the base-case parameters used in this investigation came from experimental measurements in two similar avian species, Gambel's quail and the Japanese quail. The adaptation of those parameters for use in the model is described in MATHEMATICAL MODEL. Although in most cases no further comment is merited, it is noteworthy that there is greater uncertainty in the transport parameters used for the CD system than in those used for loops of Henle. To our knowledge, the rate of active NaCl transport from avian CDs and the permeabilities to Na^+ or Cl^- have not been measured. Our basis for the base-case values used in the model (Table 2) consists of experiments that indicated that the activity of $\text{Na}^+ - \text{K}^+ - \text{ATPase}$ in rat and rabbit outer medullary CDs is about an order of magnitude less than in thick ALs and that Na^+ permeability in rabbit outer medullary CDs is $<10^{-5}$ cm/s (73). In addition, using an estimate based on experiments in Ref. 52, we have assumed in our base case and in the results of Table 5 that CD osmotic water permeability is low relative to the mammalian CD in antidiuresis.

Our base-case rate of CD inflow at the cone base depends on the assumption of relatively small rates of Na^+ transport across the CD epithelium, and the results of Table 5 are conditioned on the low CD osmotic water permeability. This base-case rate is consistent with a flow (per looped nephron) into the CD system, at the corticomedullary boundary, that is about one-tenth that of flow in a looped nephron. The parameter study for CD active Cl^- transport suggests that the base case provides a good approximation to the most likely configuration for CD inflow and transepithelial transport. However, other configurations based on more complete information may also be consistent with the measured loop of Henle parameters and measurements of urine osmolality and flow rate; it is noteworthy that in vivo studies indicate substantial Na^+ absorption rates from rat inner medullary CD, from 4.0 to 17.5 $\text{nmol} \cdot \text{cm}^{-2} \cdot \text{s}^{-1}$ (see references and discussion in Ref. 77). These considerations point to a need for further experimental elucidation of avian CD transport function.

Avian concentrating mechanism. The results of this investigation lend support to the countercurrent hy-

pothesis advanced by Skadhauge and Schmidt-Nielsen (66) and the NaCl-cycling hypothesis advanced by Nishimura et al. (51). The incorporation of measured parameters and reported anatomic features into a formal model framework produces simulated urine osmolalities that are consistent with those measured in birds. Also, the model formulation results in a simulated concentrating mechanism that operates largely through NaCl cycling from ALs to DLs. However, the model also appears to operate nearly equally well, with respect to simulated urine osmolality, in modes in which there is only NaCl cycling or only water withdrawal (modes in which thin DL water permeability or Cl^- permeability have been set to zero, respectively). This result suggests that NaCl cycling may not only serve the concentrating mechanism but may also serve other ends, notably a reduced load on medullary vascular countercurrent exchange or the return of more NaCl to the cortex via AL flow.

The model predicts that the osmolality profile produced by the avian concentrating mechanism along the medullary cone will be nearly linear, although perhaps slightly concave downward (Fig. 3), a prediction that is consistent with tissue-slice studies reported in Fig. 7 of Ref. 16. However, a conclusion that the model is consistent with these studies must be considered tentative, because the experimental sampling sites were not precisely spaced along the cone (16), and the relative locations of those sites may affect the degree and orientation of concavity (cf. curves reported in Ref. 23, Figs. 1 and 3, with curves redrawn in Ref. 63, Fig. 5). Thus additional experiments are required to more certainly determine whether the shape of the *in vivo* profile is in agreement with the model prediction.

As in models of the mammalian concentrating mechanism (43, 44, 72, 79), this model predicts that concentrating capacity is critically dependent on the CD inflow rate from the cortex. Experiments have indicated that antidiuretic states in birds are induced, at least in part, by the reduction or elimination of glomerular filtration into loopless nephrons (5, 68). The reduction in filtration results in less fluid entering the CD system, which reduces the osmotic load presented to the concentrating mechanism. The sensitivity curve shown in Fig. 7A indicates that substantial flow into the CD system from loopless nephrons is likely to induce a diuresis that results in greatly reduced concentrating capability.

A notable model prediction is that 70% of the concentrating capability arises from active NaCl absorption from the thick prebend segments of DLs (which were assumed to be nearly water impermeable). This result is consistent with findings in a previous, highly schematic model study by Layton and Davies (44), which attributed the increased concentrating capability to three factors: 1) a reduced osmotic load, since DL fluid in the prebend segment is not further concentrated, 2) a near doubling of solute absorption from the near-bend segments of each loop of Henle, where CD flow is least, relative to the extent of that loop, and 3) a cascade effect in which absorption from the loop

bends of shorter loops augments the osmolality in thin DLs of longer loops. The parameter sensitivity study for PBE length (Fig. 9) indicated that a thick DL segment up to one-third of the length of the cone would substantially increase the U/P osmolality ratio and the relative efficiency of the concentrating mechanism.

A second notable model prediction is that the decreasing loop of Henle population, as a function of medullary cone depth, is an energy-efficient configuration in terms of the amount of active NaCl absorption required to concentrate urine. Indeed, a parameter study comparing exponentially decreasing distributions of loops showed that relative efficiency decreased rapidly as the fraction of loops reaching the papillary tip increased (Fig. 10). The U/P osmolality ratio increased very rapidly, however, to ~ 2.4 as the fraction increased to 0.15, but as the fraction further increased, little was gained in the U/P osmolality ratio, which, indeed, eventually decreased.

We interpret these results as indicating that *in vivo* the number of loops of Henle is balanced with the remaining flow in CDs at each medullary level. When too many loops reach deep into the cone, the flow in the many thin DLs presents a substantive osmotic load, which is not balanced with concentrating capacity, owing to too little active NaCl absorption from thick segments in the upper portion of the cone, with absorption arising mostly from ALs and not from prebend thick segments. When too few loops reach deep into the cone, there is insufficient active absorption to effectively concentrate the flow remaining in the CDs near the cone tip.

Lessons for mammalian concentrating mechanism. Experimental studies indicate that the concentrating mechanism found in most birds is simpler than that found in most mammals. The avian mechanism depends on one solute, NaCl, and it appears to have loops of Henle that have less functional segmentation than do those of mammals. Moreover, the avian mechanism appears to operate on principles very similar to those advanced by Kuhn and Ramel (39), who in 1959 proposed that the mammalian renal countercurrent system operates by single-solute cycling based on active transport of NaCl from ALs and diffusive entry of NaCl into water-impermeable DLs. The simplicity of the avian mechanism may help us better understand the mammalian mechanism.

Avian loops of Henle most closely resemble those loops in mammals that are short-looped. Table 6 provides tubular transport parameters measured in short loops of Henle and in outer medullary CDs of several mammalian species; these may be compared with the avian parameters collected in Table 2 and used in this study. The loops of Henle of avian nephrons and short-looped mammalian nephrons share key characteristics. In both, ALs have low permeabilities to water and NaCl and are capable of vigorous active NaCl transport. These properties ensure that ALs can carry dilute fluid from deeper levels of the medulla to higher levels and from those higher levels into the cortex. This capability is a fundamental mass balance requirement

Table 6. *Outer medullary transport properties in mammalian kidneys*

Segment	P_f , $\mu\text{m/s}$	P_{Na^+} , 10^{-5} cm/s	P_{Cl^-} , 10^{-5} cm/s	$\text{Na}^+\text{-K}^+\text{-ATPase}$, $\text{pmol}\cdot\text{mm}^{-1}\cdot\text{min}^{-1}$
<i>Mouse</i>				
AL	23 (24)	2.3 (27)	1.0 (27)	62 (32)
<i>Rat</i>				
DL	2,295 (29)			2–5 (32, 74)
AL		1.1* (48)	1.1* (48)	41–139 (OS) (19)
CD				260 (IS) (19)
				11–41 (19, 74)
<i>Hamster</i>				
DL	3,257 (30)	4.8 (30)	1.5 (30)	
<i>Rabbit</i>				
DL	2,420 (38)	0–2 (1, 38, 59)		2–4 (32)
AL	0 (60)	2.8†, 6.3 (8, 60)	1.4†, 1.1 (8, 60)	41–124 (32)
CD	445‡ (28, 61)	0.39 (73)		8–19 (18, 32, 33, 65)

Numbers in parentheses indicate references. P_f , osmotic water permeability; P_{Na^+} , Na^+ permeability; P_{Cl^-} , Cl^- permeability; OS, outer stripe; IS, inner stripe. *Estimated from cortical thick AL. †OS and cortical thick AL. ‡In the presence of vasopressin.

for generating a hyperosmotic medulla (63). In the avian medullary cone and the mammalian outer medulla, no other driving mechanism is thought to contribute to the concentrating mechanism.

However, avian thin DLs have high permeability to NaCl but moderate permeability to water, while outer medullary DLs of Henle in mammals have high permeability to water but low permeability to NaCl . In accordance with avian DL permeability properties, our model study suggests that fluid in avian DLs is concentrated principally by NaCl addition. In contrast, outer medullary DL segments in mammals are thought to be concentrated principally by water withdrawal. [Recent experiments in rat, however, suggest that in the DLs of short loops of Henle, high water permeability may not continue through the inner portion of the inner stripe (75). Experimental studies in some mammals have indicated that fluid in inner medullary long DLs is also concentrated principally by water withdrawal, but there is substantial variability, depending on species and experimental conditions (62). For example, in *Psammomys obesus*, where the inner medullary concentrating mechanism appears to depend principally on NaCl , osmotic equilibration of the DLs appears to be attained principally by NaCl entry (14, 15).]

The different mode of DL concentration in birds, compared with that of DL concentration in mammalian outer medulla, leads to consideration of the first of three lessons (or implications) that this model study has for the mammalian concentrating mechanism: the high water permeability measured in mammalian DLs is not, in principle, a necessary requirement for an effective concentrating mechanism. The avian model shows that the concentration of DL fluid by solute addition can be as effective as, or even more effective than, concentration by osmotically driven water withdrawal. However, the study by Layton and Davies (44) indicated that solute addition to DLs would tend to increase the osmotic load on a distributed loop system by increasing the fluid carried by DLs, if rates of solute

absorption from ALs are assumed to be fixed. That result, taken together with this study, suggests that the predicted effectiveness of solute cycling arises from the large amount of NaCl that is made available for absorption from thick limbs of Henle.

In most mammals, urea is thought to play an important role in the inner medullary concentrating mechanism, and urea is concentrated in urine to aid in nitrogen excretion. Water absorption from outer medullary DLs would tend to increase urea concentration in tubular fluid entering downstream segments. Therefore, mammals may differ from birds in terms of the means by which the intratubular flows in outer medullary DLs are concentrated, so that mammals can more easily trap urea in the tubules and vessels of the inner medulla and so that concentrations of urea can be sufficiently high in urine to maintain a high rate of nitrogen excretion.

A second lesson for the mammalian system is that prebend enlargements are likely to play a significant role in the outer medullary and inner medullary concentrating mechanisms. Although this role has been previously hypothesized (44, 45), this study of the quail medullary cone indicates, in the context of a specific physiological setting, that the PBEs can significantly increase concentrating capability. Prebend segments have been identified in the long loops of Henle of the chinchilla; these segments have transport properties (low water permeability and high solute permeabilities) similar to thin ALs in chinchilla (13). PBEs have been reported in long loops in rats (37, 69). Short loops of Henle in rat have recently been found to have a long prebend segment that appears to be water impermeable but urea permeable (75). This segment, which is coextensive with the inner part of the inner stripe of the outer medulla, has been hypothesized to play a role in urea cycling (75), but it may also enhance concentrating capacity by removing the osmotic load that would otherwise be presented to the inner stripe by DL fluid.

A third lesson, which follows from consideration of results shown in Fig. 10, is that concentrating capacity of the loops of Henle or other elements of the mammalian inner medullary concentrating mechanism, when more fully understood, is likely to be balanced at each medullary level by the osmotic load presented by CD flow.

Renal function in dinosaurs. Many paleobiologists consider birds to be the descendants of theropod dinosaurs or to be theropod dinosaurs (53); thus study of the modern avian kidney may give insight into the renal function of extinct dinosaurs. The results of this study, by lending support to the hypothesis that birds employ a single-solute countercurrent mechanism for concentrating urine, also lend support to a similar concentrating mechanism in the extinct dinosaurs. A reasonable inference from results of this study is that the concentrating mechanism employed by birds may not provide, or may not be suited for, the production of a highly concentrated urine similar to that produced by some mammals. Because a similar inference may also apply to some extinct dinosaurs, we may also infer that some dinosaurs may have had a limited adaptability to circumstances in which water supply was limited.

Summary. This study indicates and/or predicts that 1) concentrated urine is produced in the medullary cones of the quail by a process of countercurrent multiplication that relies on NaCl transport from ALs to provide the single effect, 2) this countercurrent multiplier system employs NaCl cycling from ALs to DLs, 3) in the presence of moderate thin DL water permeability, concentrating capability is not critically dependent on NaCl cycling from ALs to DLs, 4) in the presence of sufficiently high thin DL NaCl permeability, concentrating capability is nearly independent of DL water permeability, 5) the osmolality profile along the medullary cone is nearly linear, although somewhat concave downward, 6) concentrating capability depends on an adequate DL inflow, but too much inflow results in decreased concentrating capability, 7) concentrating capability is sensitive to CD inflow, with concentrating capability rapidly diminishing as inflow increases through the physiological range, 8) active NaCl transport from the thick, prebend segments of the loops of Henle significantly increases concentrating capability, 9) the exponential decline in loop of Henle population as a function of medullary depth tends to minimize the costs of concentrating urine when assessed in terms of the number of Na⁺-K⁺-ATPase pumps required, 10) because of the need to concentrate urea in tubular fluid, most mammals may rely on water absorption, rather than solute cycling, to concentrate fluid in the DLs of the outer medulla, and 11) in mammals, prebend loop segments may augment concentrating capacity, and the decreasing loop of Henle population may help minimize the energy costs of concentrating urine.

APPENDIX

Model equations. The avian medullary cone is represented in this study by a dynamic, single-solute (Cl⁻), distributed-loop, CC model. Here we provide the equations for the model.

The medullary cone extends from the cone base, designated $x = 0$, to the cone tip, $x = L$. The indexes $i = 1, 2, 3$, and 4 designate DLs, ALs, the CD system, and the CC, respectively. With these conventions, water conservation at position x , in a DL or AL reaching to level y , is represented by

$$\frac{\partial}{\partial x} F_{iV}(x,y,t) = J_{iV}(x,y,t) \quad (A1)$$

where $i = 1$ or 2, $0 \leq x \leq y \leq L$, $F_{iV}(x,y,t)$ is the water flow rate in the tubule at time t , and $J_{iV}(x,y,t)$ is the transepithelial water line flux, i.e., the water transport rate per unit tubular length, taken positive for transport into the tubule.

Cl⁻ conservation at x , in a DL or AL reaching to level y , is represented by

$$\frac{\partial}{\partial t} C_i(x,y,t) = -\frac{1}{A_i(x,y)} \left[F_{iV}(x,y,t) \frac{\partial}{\partial x} C_i(x,y,t) - J_{iS}(x,y,t) + C_i(x,y,t) J_{iV}(x,y,t) \right] \quad (A2)$$

where $i = 1$ or 2, $0 \leq x \leq y \leq L$, $C_i(x,y,t)$ is Cl⁻ concentration at x and time t , $A_i(x,y)$ is the cross-sectional area of the tubule, and $J_{iS}(x,y,t)$ is the transepithelial line flux of Cl⁻, taken positive for transport into the tubule. The three terms on the right represent effects of axial intratubular Cl⁻ advection, transepithelial Cl⁻ transport, and transepithelial water transport, respectively. The first and third of these terms arise from the space derivative of the axial Cl⁻ advection rate (or mass flow rate), $F_{iV}C_i$. In *Eqs. A1* and *A2* and in similar equations to follow, we assume that water volume is unaffected by solute present in small concentrations. A derivation for these well-known equations may be found elsewhere (46); the only difference here is the use of line fluxes rather than fluxes based on tubular area. The use of line fluxes simplifies the formulation of the conservation equations for the CC (*Eqs. A5* and *A6*).

The transepithelial water line flux in a DL or AL is given by

$$J_{iV}(x,y,t) = 2\pi r_i(x,y) \bar{V}_w P_{fi}(x,y) \phi \sigma_i(x,y) [C_i(x,y,t) - C_4(x,t)] \quad (A3)$$

where $r_i(x,y)$ is the radius of the tubule, \bar{V}_w is the partial molar volume of water, $P_{fi}(x,y)$ is the osmotic water permeability coefficient at x for a loop turning at y , ϕ is the osmotic coefficient of NaCl, $\sigma_i(x,y)$ is the reflection coefficient of Cl⁻, and $C_4(x,t)$ is the CC concentration of Cl⁻ at x . In *Eq. A3*, ϕ and σ_i are dimensionless parameters, with $\phi = 1.84$ (76) and with $0 \leq \sigma_i \leq 1$. We assume that $\sigma_i \equiv 1$ for all tubules ($i = 1, 2, 3$, or 4).

The transepithelial Cl⁻ line flux in a DL or AL is given by

$$J_{iS}(x,y,t) = -2\pi r_i(x,y) \left(P_i(x,y) [C_i(x,t) - C_4(x,y,t)] + \frac{V_{\max,i}(x,y) C_i(x,y,t)}{K_{m,i}(x,y) + C_i(x,y,t)} \right) \quad (A4)$$

The first term on the right is transepithelial diffusion characterized by permeability $P_i(x,y)$. The second term on the right arises from metabolically driven active transport characterized by Michaelis-Menten kinetics with Michaelis constant $K_{m,i}(x,y)$ and maximum transport rate per unit tubular area, $V_{\max,i}(x,y)$. The negative sign for this term reflects the

assumption that active transport will generally be directed out from the tubule. Because all reflection coefficients are assumed equal to unity, no term appears for solvent drag.

The CD system and CC are represented by single tubes with decreasing cross-sectional areas. The conservation equations for these tubes are analogous to *Eqs. A1* and *A2* but depend on only one space variable x extending from $x = 0$ to $x = L$

$$\frac{\partial}{\partial x} F_{iV}(x,t) = J_{iV}(x,t) \tag{A5}$$

and

$$\begin{aligned} \frac{\partial}{\partial t} C_i(x,t) = & \\ & - \frac{1}{A_i(x)} \left[F_{iV}(x,t) \frac{\partial}{\partial x} C_i(x,t) - J_{iS}(x,t) + C_i(x,t) J_{iV}(x,t) \right] \end{aligned} \tag{A6}$$

where $i = 3$ or 4 . The flux equations for the CD system are given by

$$J_{3V}(x,t) = 2\pi r_3(x) \bar{V}_w P_{f,3}(x) \phi \sigma_3(x) [C_3(x,t) - C_4(x,t)] \tag{A7}$$

and

$$\begin{aligned} J_{3S}(x,t) = & \\ & - 2\pi r_3(x) \left(P_3(x) [C_3(x,t) - C_4(x,t)] + \frac{V_{\max,3}(x) C_3(x,t)}{K_{m,3}(x) + C_3(x,t)} \right) \end{aligned} \tag{A8}$$

In our model formulation, the radius $r_3(x)$ in these equations includes scalings for the change in CD radius as a function of medullary depth, the coalescences of CDs, and the ratio of CDs at the cone base to loops of Henle at the cone base. Thus transport from the CD system is scaled to give fluxes at level x per looped nephron entering the cone base (see below).

For the CC, the transepithelial fluxes arise from the fluxes already defined for the loops of Henle and the CD system. However, in the case of the loops of Henle, the fluxes must be weighted according to the loop distribution $w(x)$, which is the fraction of loops reaching to level x .

Experimental results indicate that the fraction of loops reaching depth x in the avian cone can be approximated by a decreasing exponential function with a step jump to zero at the cone tip (11). Thus

$$w(x) = \begin{cases} e^{-dx/L}, & x \in [0, L] \\ 0, & x > L \end{cases} \tag{A9}$$

where $d > 0$. Let $H_L(x)$ denote the translated Heaviside function that is equal to 1 for $x > L$ and equal to zero otherwise. Then the function w given in *Eq. A9* can be written as

$$w(x) = e^{-dx/L} [1 - H_L(x)], \quad x \geq 0 \tag{A10}$$

In the sense of distributions (67), this function has a derivative given by

$$w'(x) = -e^{-dx/L} \delta_L(x) - (d/L)w(x), \quad x \geq 0 \tag{A11}$$

where δ_L is the Dirac delta measure with support at $x = L$ only and the rightmost term applies for $x \neq L$. This derivative is equivalent to

$$w'(x) = \begin{cases} -(d/L)e^{-dx/L}, & x \in [0, L) \\ -e^{-d} \delta_L(x), & x = L \\ 0, & x > L \end{cases} \tag{A12}$$

For $i = 1$ or 2 and for k designating Cl^- ($k = S$) or water ($k = V$), we define composite (or total) transepithelial fluxes, per looped nephron, for the limbs of the loops of Henle by

$$\begin{aligned} J_{ik}(x,t) &= \lim_{\epsilon \downarrow 0} \int_x^{L+\epsilon} J_{ik}(x,y,t) [-w'(y)] dy \\ &= \lim_{\epsilon \downarrow 0} \int_x^{L-\epsilon} J_{ik}(x,y,t) [-w'(y)] dy + e^{-d} J_{ik}(x,L,t) \end{aligned} \tag{A13}$$

In *Eqs. A13* the downward-directed arrows indicate that the positive quantity ϵ is decreasing toward zero. Both equations represent the total Cl^- or water efflux at cone depth x from DLs or ALs reaching to at least cone depth x , and both include the contribution at level x from loops that reach to the cone tip. In the second of *Eqs. A13*, the contribution from loops reaching the cone tip is exhibited as a separate term (the rightmost term) through the action of the Dirac delta measure at $x = L$.

By using the specifications of $J_{1k}(x,t)$ and $J_{2k}(x,t)$ given by *Eqs. A13*, the sum of the line fluxes into the CC can be expressed by

$$J_{4k}(x,t) = -[J_{1k}(x,t) + J_{2k}(x,t) + J_{3k}(x,t)] \tag{A14}$$

where we distinguish composite fluxes $J_{ik}(x,t)$ from single-tubule fluxes $J_{ik}(x,y,t)$ by writing out their arguments and where $k = S$ or V .

Because the CC is assumed closed at the tip of the medullary cone, there is no advective entry of solute or fluid at $x = L$. Therefore, the solute concentration at $x = L$, instead of satisfying a PDE of the form of *Eq. A6*, must satisfy the ordinary differential equation

$$\frac{\partial}{\partial t} C_4(L,t) = -\frac{1}{A_4(L)} [-J_{4S}(L,t) + C_4(L,t) J_{4V}(L,t)] \tag{A15}$$

For the equations formulated for the DLs and ALs, boundary conditions must be specified at the base of the cone and at loop bends. Thus, for the DLs, $F_{1V}(0,y,t)$ and $C_1(0,y,t)$ must be specified. At a loop bend the DL is continuous with the AL. Thus, $C_2(x,x,t) = C_1(x,x,t)$, and $F_{2V}(x,x,t) = -F_{1V}(x,x,t)$, where the negative sign arises because flow is taken positive in the increasing x direction. The boundary conditions for the CD system are $F_{3V}(0,t)$ and $C_3(0,t)$. Since the weight w scales the aggregate fluxes $J_{ik}(x,t)$ from loops of Henle ($i = 1$ or 2) in terms of flux per looped nephron at the cone base, it is natural and convenient to express $F_{3V}(0,t)$ in terms of CD flow per looped nephron and to scale the CD fluxes accordingly in *Eqs. A7* and *A8*.

The initial concentrations are $C_i(x,y,t)$ for $i = 1$ or 2 and $C_i(x,t)$ for $i = 3$ or 4 . Since the tubes are assumed rigid, the analogous initial axial water flows F_{iV} are computed from the initial transtubular water fluxes, which arise from the initial concentrations already specified.

The total active Cl^- transport rate from thick limbs of Henle (TAT) is computed by integrating over the aggregate loops of Henle as follows. Let $J_i^A(x,y,t)$ represent the rate of active transport from an individual DL ($i = 1$) or AL ($i = 2$). Then, retaining only the Michaelis-Menten term from *Eq. A4*, one obtains

$$J_i^A(x,y,t) = -2\pi r_i(x,y) \frac{V_{\max,i}(x,y) C_i(x,y,t)}{K_{m,i}(x,y) + C_i(x,y,t)} \tag{A16}$$

The rate of solute flux from the aggregate DLs or ALs, $J_i^A(x,t)$, is given by an equation analogous to the second of *Eqs. A13* per looped nephron

$$J_i^A(x,t) = \lim_{\epsilon \downarrow 0} \int_x^{L-\epsilon} J_i^A(x,y,t)[-w'(y)] dy + e^{-d} J_i^A(x,L,t) \quad (A17)$$

Then, for all loops of Henle, throughout the medulla, we have that the total rate of active transport at time t , per looped nephron is given by

$$\text{TAT}(t) = \int_0^L [J_1^A(x,t) + J_2^A(x,t)] dx \quad (A18)$$

Note that TAT is total active transport, and not net transport, which would involve terms for transepithelial Cl^- diffusion. Also, in this study, all calculations were conducted to obtain steady states, so no dependent variable, as reported in RESULTS, depends on time t , and thus TAT does not depend on t .

Quantities defined above can be related to the level curves given in Fig. 4: A corresponds to $2r_i(x,y)$, B corresponds to $C_i(x,y,ss)$, C corresponds to $F_{iV}(x,y,ss)$, and D corresponds to $F_{iS}(x,y,ss)$. In these functions, $i = 1$ or 2 for DLs or ALs, respectively, and the time variable t has been replaced with ss to indicate a steady state. Each function of this type represents a quantity at level x in a limb of a loop of Henle with bend at level y ; thus $0 \leq x \leq y \leq L$. To explain the relationship of the model functions to the graphs in Fig. 4, let h and v represent the horizontal and vertical axes, respectively, in Fig. 4, $A-D$, and suppose that h and v are fractional, each ranging from 0 to 1, rather than percentages. Let the origin $(0,0)$ for the coordinates (h,v) correspond to the lower left corner of Fig. 4, $A-D$. Then, in Fig. 4A, the lower left triangle represents the DL diameters $2r_1(hL, (1-v)L)$ (with the constraint $h \leq 1-v$), and the upper right triangle represents the AL diameters $2r_2((1-v)L, hL)$ (with the constraint $v \leq h$). Analogous expressions apply for functions represented in Fig. 4, $B-D$. Thus, for presentation in the format of Fig. 4, the second coordinate of each function for the DLs was rescaled, and the abscissa and ordinate were reversed when passing from each function representing DLs to each function representing ALs.

We thank Kayne M. Arthurs for assistance with final figure preparation and Leon C. Moore for comments and suggestions, which led to improvements in the analysis and presentation of model results.

This work was principally supported by National Institute of Diabetes and Digestive and Kidney Diseases Grant DK-42091 to H. E. Layton. Additional support was provided by the National Science Foundation through Group Infrastructure Grant DMS-9709608 to M. C. Reed, H. E. Layton, and J. J. Blum and through Grants DMS-9709608, IBN-9220241, and IBN-9515450 to E. J. Braun.

Portions of this work were completed while H. E. Layton was on sabbatical leave at the Institute for Mathematics and Its Applications at the University of Minnesota, Minneapolis, MN.

This work was presented at Experimental Biology '97 and has been published in abstract form (*FASEB J* 11: A9, 1997).

REFERENCES

1. **Abramov M and Orci L.** On the "tightness" of the rabbit descending limb of the loop of Henle—physiological and morphological evidence. *Int J Biochem* 12: 23–27, 1980.
2. **Beuchat CA.** Body size, medullary thickness, and urine concentrating ability in mammals. *Am J Physiol Regulatory Integrative Comp Physiol* 258: R298–R308, 1990.
3. **Boykin SLB and Braun EJ.** Entry of nephrons into the collecting duct network of the avian kidney: a comparison of chickens and desert quail. *J Morphol* 216: 259–269, 1993.
4. **Braun EJ.** Renal function in birds. In: *New Insights in Vertebrate Kidney Function*, edited by Brown JA, Balment RJ, and Rankin JC. Cambridge, UK: Cambridge University Press, 1993, p. 167–188.
5. **Braun EJ and Dantzler WH.** Function of mammalian-type and reptilian-type nephrons in kidney of desert quail. *Am J Physiol* 222: 617–629, 1972.
6. **Braun EJ and Reimer PR.** Structure of avian loop of Henle as related to countercurrent multiplier system. *Am J Physiol Renal Fluid Electrolyte Physiol* 255: F500–F512, 1988.
7. **Braun EJ, Reimer PR, and Pacelli MM.** The nature of uric acid in avian urine (Abstract). *Physiologist* 30: 120, 1987.
8. **Burg MB and Green N.** Function of the thick ascending limb of Henle's loop. *Am J Physiol* 224: 659–668, 1973.
9. **Casotti G, Beauchat CA, and Braun EJ.** Morphology of the kidney in a nectarivorous bird, the Anna's hummingbird *Calypte anna*. *J Zool Lond* 244: 175–184, 1998.
10. **Casotti G and Braun EJ.** Ionic composition of urate-containing spheres in the urine of domestic fowl. *Comp Biochem Physiol A Physiol* 118: 585–588, 1997.
11. **Casotti G, Lindberg KK, and Braun EJ.** Functional morphology of the avian medullary cone. *Am J Physiol Regulatory Integrative Comp Physiol*. In press.
12. **Chou C-L, Knepper MA, and Layton HE.** Urinary concentrating mechanism: the role of the inner medulla. *Semin Nephrol* 13: 168–181, 1993.
13. **Chou C-L, Nielsen S, and Knepper MA.** Structural-functional correlation in chinchilla long loop of Henle thin limbs: a novel papillary subsegment. *Am J Physiol Renal Fluid Electrolyte Physiol* 265: F863–F874, 1993.
14. **De Rouffignac C.** The urinary concentrating mechanism. In: *Urinary Concentrating Mechanisms. Comparative Physiology*, edited by Kinne RKH. Basel: Karger, 1990, vol. 2, p. 31–103.
15. **De Rouffignac C and Morel F.** Micropuncture study of water, electrolytes and urea movements along the loops of Henle in *Psammomys*. *J Clin Invest* 48: 474–486, 1969.
16. **Emery N, Poulson TL, and Kinter WB.** Production of concentrated urine by avian kidneys. *Am J Physiol* 223: 180–187, 1972.
17. **Gamble JL, McKhann CF, Butler AM, and Tuthill E.** An economy of water in renal function referable to urea. *Am J Physiol* 109: 139–154, 1934.
18. **Garg LC, Knepper MA, and Burg MB.** Mineralocorticoid effects on Na-K-ATPase in individual nephron segments. *Am J Physiol Renal Fluid Electrolyte Physiol* 240: F536–F544, 1981.
19. **Garg LC, Mackie S, and Tischer CC.** Effect of low potassium diet on Na-K-ATPase in rat nephron segments. *Pflügers Arch* 394: 113–117, 1982.
20. **Goldstein DL and Braun EJ.** Structure and concentrating ability in the avian kidney. *Am J Physiol Regulatory Integrative Comp Physiol* 256: R501–R509, 1989.
21. **Greger R.** Chloride reabsorption in the rabbit cortical thick ascending limb of the loop of Henle. A sodium dependent process. *Pflügers Arch* 390: 38–43, 1981.
22. **Greger R and Velázquez H.** The cortical thick ascending limb and early distal convoluted tubule in the concentrating mechanism. *Kidney Int* 31: 590–596, 1987.
23. **Hai MA and Thomas S.** The time-course of changes in renal tissue composition during lysine vasopressin infusion in the rat. *Pflügers Arch* 310: 297–319, 1969.
24. **Hall DA and Varney DM.** Effect of vasopressin in electrical potential differences and chloride transport in mouse medullary thick ascending limb of Henle. *J Clin Invest* 66: 792–802, 1980.
25. **Han JS, Thompson KA, Chou C-L, and Knepper MA.** Experimental tests of three-dimensional model of urinary concentrating mechanism. *J Am Soc Nephrol* 2: 1677–1688, 1992.
26. **Hargitay B and Kuhn W.** Das Multiplikationsprinzip als Grundlage der Harnkonzentrierung in der Niere. *Z Elektrochem* 55: 539–558, 1951.
27. **Hebert SC, Culpepper RM, and Andreoli TE.** NaCl transport in mouse medullary thick ascending limbs. I. Functional nephron heterogeneity and ADH-stimulated NaCl cotransport. *Am J Physiol Renal Fluid Electrolyte Physiol* 241: F412–F431, 1981.

28. **Horster MF and Zink H.** Functional differentiation of the medullary collecting tubule: influence of vasopressin. *Kidney Int* 22: 360–365, 1982.
29. **Imai M.** Function of the thin ascending limb of Henle of rats and hamsters perfused in vivo. *Am J Physiol Renal Fluid Electrolyte Physiol* 232: F201–F209, 1977.
30. **Imai M, Hayashi M, and Araki M.** Functional heterogeneity of the descending limbs of Henle's loop. I. Internephron heterogeneity in the hamster kidney. *Pflügers Arch* 402: 385–392, 1984.
31. **Johnson OW.** Urinary organs. In: *Form and Function in Birds*, edited by King AS and McLelland J. New York: Academic, 1979, vol. 1, p. 183–235.
32. **Katz AI.** Distribution and function of classes of ATPases along the nephron. *Kidney Int* 29: 21–31, 1986.
33. **Katz AI, Doucet A, and Morel F.** Na-K-ATPase activity along the rabbit, rat and mouse nephron. *Am J Physiol Renal Fluid Electrolyte Physiol* 237: F114–F120, 1979.
34. **Kellogg RB.** Some singular perturbation problems in renal models. *J Math Anal Appl* 128: 214–240, 1987.
35. **Knepper MA.** Measurement of osmolality in kidney slices using vapor pressure osmometry. *Kidney Int* 21: 653–655, 1982.
36. **Knepper MA, Danielson RA, Saidel GM, and Post RS.** Quantitative analysis of renal medullary anatomy in rats and rabbits. *Kidney Int* 12: 313–323, 1977.
37. **Koepsell H, Kriz W, and Schnermann J.** Pattern of luminal diameter changes along the descending and ascending thin limbs of the loop of Henle in the inner medullary zone of the rat kidney. *Z Anat Entwicklungsgesch* 138: 321–328, 1972.
38. **Kokko JP.** Sodium chloride and water transport in the descending limb of Henle. *J Clin Invest* 49: 1838–1846, 1970.
39. **Kuhn W and Ramel A.** Aktiver Salztransport als möglicher (und wahrscheinlicher) Einzeleffekt bei der Harnkonzentrierung in der Niere. *Helv Chim Acta* 42: 628–660, 1959.
40. **Kuhn W and Ryffel K.** Herstellung konzentrierter Lösungen aus verdünnten durch bloße Membranwirkung: ein Modellversuch zur Funktion der Niere. *Hoppe-Seyler's Z Physiol Chem* 276: 145–178, 1942.
41. **Laverty G and Dantzer WH.** Micropuncture of superficial nephrons in avian (*Sturnus vulgaris*) kidney. *Am J Physiol Renal Fluid Electrolyte Physiol* 243: F561–F569, 1982.
42. **Layton HE.** Distribution of Henle's loops may enhance urine concentrating capability. *Biophys J* 49: 1033–1040, 1986.
43. **Layton HE.** Urea transport in a distributed loop model of the urine concentrating mechanism. *Am J Physiol Renal Fluid Electrolyte Physiol* 258: F1110–F1124, 1990.
44. **Layton HE and Davies JM.** Distributed solute and water reabsorption in a central core model of the renal medulla. *Math Biosci* 116: 169–196, 1993.
45. **Layton HE, Knepper MA, and Chou C-L.** Permeability criteria for effective function of passive countercurrent multiplier. *Am J Physiol Renal Fluid Electrolyte Physiol* 270: F9–F20, 1996.
46. **Layton HE and Pitman EB.** A dynamic numerical method for models of renal tubules. *Bull Math Biol* 56: 547–565, 1994.
47. **Layton HE, Pitman EB, and Knepper MA.** A dynamic numerical method for models of the urine concentrating mechanism. *SIAM J Appl Math* 5: 1390–1418, 1995.
48. **Mason J, Gutsche H-U, Moore L, and Müller-Suur R.** The early phase of experimental acute renal failure. IV. The diluting ability of the short loops of Henle. *Pflügers Arch* 379: 11–18, 1979.
49. **Miwa T and Nishimura H.** Diluting segment in avian kidney. II. Water and chloride transport. *Am J Physiol Regulatory Integrative Comp Physiol* 250: R341–R347, 1986.
50. **Nishimura H, Imai M, and Ogawa M.** Diluting segment in avian kidney. I. Characterization of transepithelial voltages. *Am J Physiol Regulatory Integrative Comp Physiol* 250: R333–R340, 1986.
51. **Nishimura H, Koseki C, Imai M, and Braun EJ.** Sodium chloride and water transport in the thin descending limb of Henle of the quail. *Am J Physiol Renal Fluid Electrolyte Physiol* 257: F994–F1002, 1989.
52. **Nishimura H, Koseki C, and Patel TB.** Water transport in collecting ducts of Japanese quail. *Am J Physiol Regulatory Integrative Comp Physiol* 271: R1535–R1543, 1996.
53. **Padian KC and Chiappe LM.** The origin and early evolution of birds. *Biol Rev* 73: 1–42, 1998.
54. **Pallone TL.** Effect of sodium chloride gradients on water flux in rat descending vasa recta. *J Clin Invest* 87: 12–19, 1991.
55. **Pallone TL.** Transport of sodium chloride and water in rat ascending vasa recta. *Am J Physiol Renal Fluid Electrolyte Physiol* 261: F519–F525, 1991.
56. **Pallone TL.** The extraglomerular microcirculation of the kidney. In: *The Kidney: Physiology and Pathophysiology* (3rd ed.), edited by Seldin DW and Giebisch G. Philadelphia, PA: Lippincott, Williams & Wilkins, 2000, p. 791–822.
57. **Pallone TL, Work J, and Jamison RL.** Resistance of descending vasa recta to the transport of water. *Am J Physiol Renal Fluid Electrolyte Physiol* 259: F688–F697, 1990.
58. **Pallone TL, Work J, Myers RL, and Jamison RL.** Transport of sodium and urea in outer medullary descending vasa recta. *J Clin Invest* 93: 212–222, 1994.
59. **Rocha AS and Kokko JP.** Membrane characteristics regulating potassium transport out of the isolated perfused descending limb of Henle. *Kidney Int* 4: 326–330, 1973.
60. **Rocha AS and Kokko JP.** Sodium chloride and water transport in the medullary thick ascending limb of Henle. Evidence for active chloride transport. *J Clin Invest* 52: 612–623, 1973.
61. **Rocha AS and Kokko JP.** Permeability of medullary nephron segments to urea and water: effect of vasopressin. *Kidney Int* 6: 379–387, 1974.
62. **Roy, DR Jr, Layton HE, and Jamison RL.** Countercurrent mechanism and its regulation. In: *The Kidney: Physiology and Pathophysiology* (2nd ed.), edited by Seldin DW and Giebisch G. New York: Raven, 1992, p. 1649–1692.
63. **Sands JM and Layton HE.** Urine concentrating mechanism and its regulation. In: *The Kidney: Physiology and Pathophysiology* (3rd ed.), edited by Seldin DW and Giebisch G. Philadelphia, PA: Lippincott, Williams & Wilkins, 2000, p. 1175–1216.
64. **Sasaki Y, Takahashi T, and Suwa N.** Quantitative structural analysis of the inner medulla of rabbit kidney. *Tohoku J Exp Med* 98: 21–32, 1969.
65. **Schmidt U and Horster M.** Na-K-activated ATPase: activity maturation in rabbit nephron segments dissected in vitro. *Am J Physiol Renal Fluid Electrolyte Physiol* 233: F44–F60, 1977.
66. **Skadhauge E and Schmidt-Nielsen B.** Renal medullary electrolyte and urea gradient in chickens and turkeys. *Am J Physiol* 212: 1313–1318, 1967.
67. **Stakgold I.** *Green's Functions and Boundary Value Problems* (2nd ed.). New York: Wiley, 1998.
68. **Stallone JN and Braun EJ.** Contributions of glomerular and tubular mechanisms to antidiuresis in conscious domestic fowl. *Am J Physiol Renal Fluid Electrolyte Physiol* 249: F842–F850, 1985.
69. **Steinhausen M.** In vivo-Beobachtungen an der Nierenpapille von Goldhamstern nachintravenöser Lissamingrün-Injektion. *Pflügers Arch* 279: 195–213, 1964.
70. **Stephenson JL.** Concentration of urine in a central core model of the renal counterflow system. *Kidney Int* 2: 85–94, 1972.
71. **Stephenson JL, Wang H, and Tewarson RP.** Effect of vasa recta flow on concentrating ability of models of the renal inner medulla. *Am J Physiol Renal Fluid Electrolyte Physiol* 268: F698–F709, 1995.
72. **Stephenson JL, Zhang Y, and Tewarson R.** Electrolyte, urea, and water transport in a two-nephron central core model of the renal medulla. *Am J Physiol Renal Fluid Electrolyte Physiol* 257: F399–F413, 1989.
73. **Stokes JB.** Sodium and potassium transport across the cortical and outer medullary collecting duct tubule of the rabbit: evidence for diffusion across the outer medullary portion. *Am J Physiol Renal Fluid Electrolyte Physiol* 242: F514–F520, 1982.
74. **Terada Y and Knepper MA.** Na⁺-K⁺-ATPase activities in renal tubule segments of rat inner medulla. *Am J Physiol Renal Fluid Electrolyte Physiol* 256: F218–F223, 1989.
75. **Wade JB, Lee AJ, Liu J, Ecelbarger CA, Mitchell C, Bradford AD, Terris J, Kim G-H, and Knepper MA.** UT-A2: a 55-kDa urea transporter in thin descending limb whose abun-

- dance is regulated by vasopressin. *Am J Physiol Renal Physiol* 278: F52–F62, 2000.
76. **Weast RC** (Editor). *Handbook of Chemistry and Physics* (55th ed.). Cleveland, OH: CRC, 1974.
77. **Weinstein AM**. A mathematical model of the inner medullary collecting duct of the rat: pathways for Na and K transport. *Am J Physiol Renal Physiol* 274: F841–F855, 1998.
78. **Wexler AS, Kalaba RE, and Marsh DJ**. Three-dimensional anatomy and renal concentrating mechanism. I. Modeling results. *Am J Physiol Renal Fluid Electrolyte Physiol* 260: F368–F383, 1991.
79. **Wexler AS, Kalaba RE, and Marsh DJ**. Three-dimensional anatomy and renal concentrating mechanism. II. Sensitivity results. *Am J Physiol Renal Fluid Electrolyte Physiol* 260: F384–F394, 1991.
80. **Williams JB, Pacelli MM, and Braun EJ**. The effect of water deprivation on renal function in conscious unrestrained Gambel's quail (*Callipepla gambelii*). *Physiol Zool* 64: 1200–1216, 1991.

